Am J Cancer Res 2025;15(5):2353-2374
www.ajcr.us /ISSN:2156-6976/ajcr0162718

Original Article

Circular RNA hsa_circ_103089 modulates metabolic glycolysis and influences migration, invasion, and cisplatin sensitivity in non-small cell lung cancer cells via the miR-876-5p/EGFR axis

Yong Zhou[1,2], Xiaoxiao Zhu[2], Zhongkai Tong[2], Cenli Wang[3], Xiaofei Liang[3], Zhenyan Li[3], Lin He[3], Chunli Wu[2], Zhaoxing Dong[2]

[1]School of Medicine, Tongji University, Shanghai 200092, China; [2]Department of Respiratory and Critical Care Medicine, Ningbo No. 2 Hospital, Ningbo 315000, Zhejiang, China; [3]Department of Respiratory and Critical Care Medicine, Xiangshan Red Cross Taiwan Compatriot Hospital Medical and Health Group, Ningbo 315000, Zhejiang, China

Received December 16, 2024; Accepted May 6, 2025; Epub May 25, 2025; Published May 30, 2025

Abstract: Lung cancer, particularly non-small cell lung cancer (NSCLC), remains a leading cause of cancer-related mortality worldwide, driven by complex molecular mechanisms including metabolic reprogramming and chemoresistance. Circular RNAs (circRNAs) have emerged as key regulators in cancer progression, yet their specific roles in NSCLC are underexplored. This study identified hsa_circ_103089 as a novel circRNA upregulated in NSCLC tissues and cell lines through circRNA profiling using the Gene Expression Omnibus (GEO) database. We aimed to investigate its functional roles and molecular mechanisms in NSCLC progression and cisplatin (DDP) sensitivity. Using A549 and HCC827 cell lines, we assessed the effects of hsa_circ_103089 silencing on proliferation, migration, invasion, glycolysis, and DDP resistance via techniques such as dual-luciferase reporter assays, RNA pull-down, Western blotting, and in vivo xenograft models. Results revealed that hsa_circ_103089 silencing suppressed tumor cell malignancy and glycolysis while enhancing DDP sensitivity. Mechanistically, hsa_circ_103089 acts as a sponge for miR-876-5p, upregulating EGFR expression and downstream glycolysis-related genes (e.g., LDHA, HK2, GLUT1). In vivo, hsa_circ_103089 knockdown inhibited tumor growth and potentiated DDP efficacy in nude mice. Clinically, high hsa_circ_103089 expression correlated with poor prognosis in NSCLC patients. These findings establish hsa_circ_103089 as a critical regulator of NSCLC progression and chemoresistance via the miR-876-5p/EGFR axis, highlighting its potential as a prognostic biomarker and therapeutic target.

Keywords: hsa_circ_103089, non-small cell lung cancer (NSCLC), miR-876-5p/EGFR axis, glycolysis, cisplatin resistance

Introduction

Lung cancer remains the most prevalent and deadly form of cancer, posing a profound threat to global health [1]. The current mainstays of treatment, including surgery, radiation therapy, and chemotherapy, have shown limited success [2], with a 5-year survival rate that hovers at only 22% due to high rates of metastasis and recurrence [3]. Therefore, understanding the molecular mechanisms driving lung cancer progression may facilitate the development of more precise and targeted therapeutic strategies. Reprogramming glucose metabolism is a hallmark of lung cancer, enhancing cellular proliferation, migration, and invasion [4, 5]. Glucose metabolism undergoes reprogramming, and aberrant metabolism is a significant characteristic of cancer cells, particularly aerobic glycolysis, also known as the "Warburg effect", in which tumor cells preferentially use glycolysis for energy production even in oxygen-rich conditions [6]. In cancer cells, aerobic glycolysis can convert up to 85% of glucose into lactate [7], significantly increasing the glucose consumption of lung cancer cells and providing the energy needed for their high proliferation rates [8, 9]. Previous studies have report-

https://doi.org/10.62347/PXHT9575

ed that lung cancer patients typically exhibit an abnormal increase in glycolytic pathways [4]. Monitoring changes in glycolytic pathways can be beneficial for predicting overall survival rates in lung cancer patients [10, 11].

As a subclass of non-coding RNAs (ncRNAs), circular RNAs (circRNAs) have a covalently closed loop structure. As bioinformatics technology has advanced, circRNAs' molecular processes in lung cancer have been thoroughly investigated. In this study, we conducted a comprehensive bioinformatics analysis of circRNA expression patterns in lung cancer using datasets from the Gene Expression Omnibus (GEO), specifically GSE158695 and GSE112214. Among the identified circRNAs, we focused on hsa_circ_103089, a previously unreported circRNA originating from the PCSK6 transcript. Given its high abundance and aberrant upregulation in lung cancer patients, we sought to investigate its role and downstream regulatory mechanisms in non-small cell lung cancer (NSCLC). We examined the biological functions of hsa_circ_103089, including its effects on proliferation, migration, and invasion, as well as its potential role in metabolic reprogramming in NSCLC.

Materials and methods

Clinical samples

From January 2024 to November 2024, this study collected 30 pairs of NSCLC tissue specimens from the Ningbo No. 2 Hospital. The study was approved by the Ethics Committee of Ningbo No. 2 Hospital. The informed consent form was obtained from patients before inclusion in the study, and the research procedures were fully explained. No subjects had received any form of anticancer treatment, such as chemotherapy or radiotherapy, before surgical resection. Additionally, the expression of hsa_circ_103089 was detected in NSCLC patient tissue microarrays (HLugA180Su09, Shanghai Outdo Biotech, 94 cases of lung adenocarcinoma with survival data: 94 cancer sites/86 adjacent cancer sites, with a follow-up period of 3-8 years) using Fluorescence in situ hybridization (FISH) assay. Correlations were established with clinicopathological features and the prognosis of patients.

Cell culture

Human NSCLC cell lines A549 and HCC827 were procured from Zhejiang Ruyao Biotechnology Co., Ltd. (Ningbo, China). The cells were cultured in Dulbecco's Modified Eagle Medium (DMEM) supplemented with 10% Fetal Bovine Serum (FBS), 1% penicillin, and 1% streptomycin (all from Thermo Fisher Scientific, Waltham, MA, USA). The cells were maintained in an incubator at 37°C with a CO_2 concentration of 5%. To assess the stability of circRNA, actinomycin D (A9415, Sigma Aldrich, USA) at a concentration of 5 μg/mL was added to the cells at 0, 6, 12, 18, and 24 h before RNA extraction. Subsequently, RNA was harvested to evaluate the expression levels of hsa_circ_103089 and its cognate linear transcript, PCSK6 [12].

Bioinformatics analysis

We obtained two datasets containing circRNA expression profiles from NSCLC and adjacent normal tissues (GSE158695 and GSE112214) from the GEO database (https://www.ncbi.nlm.nih.gov/geo/). The datasets were filtered using *P*_value < 0.05 and Log_FoldChange (LogFC) > 1 criteria to identify differentially expressed circRNAs. Venn diagram analysis was applied to select the target circRNAs that were significantly upregulated and highly expressed in NSCLC. Quantitative real-time reverse transcription polymerase chain reaction (qRT-PCR) was used to assess the expression levels of hsa_circ_103089 in RNA samples from Beas-2b, A549, HCC827, H1299, and Calu-1 cell lines. A549 and HCC827 cell lines, which exhibited high expression levels of hsa_circ_103089, were chosen for knockdown experiments to elucidate the biological functions of hsa_circ_103089 in NSCLC.

The base sequence of hsa_circ_103089 was utilized to predict potential downstream targets using the miRDB website. This was supplemented with an analysis of significantly downregulated miRNAs in NSCLC patients from the GEO database (GSE29250) using a *P*_value < 0.01 and LogFC < -1. Venn diagram analysis was conducted to intersect the predicted targeted miRNAs of hsa_circ_103089 with the downregulated miRNAs to identify candidate miRNAs.

The Encyclopedia of RNA Interactomes (ENCORI) database (https://rnasysu.com/encori/index.php), which integrates seven miRNA prediction databases including PITA, miRmap, microT, miRanda, PicTar, and TargetScan, was employed to predict mRNA targets of miR-876-

5p. Additionally, significantly upregulated miRNAs in NSCLC patients (GSE29250) were retrieved from the GEO database with a *P*_value < 0.01 and LogFC > 1. The GeneCard database was queried to obtain the TOP200 genes associated with glycolysis. Venn diagrams were used to filter and identify mRNAs targeted by miR-876-5p that are also closely related to glycolysis.

qRT-PCR

Total RNA was extracted from tissues or cells using TRIzol reagent (15596026CN, Invitrogen, USA). Before reverse transcription into complementary DNA (cDNA) using the PrimeScript™ RT Reagent Kit (RR047Q, Takara, Japan), RNA was incubated with RNase R for 15 min. qPCR was conducted on an ABI 7500 PCR system (Applied Biosystems, USA) with BeyoFast™ SYBR Green qPCR Mix (D7260, Beyotime, China) to amplify target mRNAs and miRNAs and measure their expression levels. For miR-876-5p, U6 small nuclear RNA and GAPDH (for hsa_circ_103089, PCSK6, and linear mRNA) were employed as endogenous reference genes. The expression levels of the target genes were determined using the $2^{-\Delta\Delta Ct}$ method. The sequences of the primers are listed below: hsa_circ_103089: Forward 5'-AAC TGA CCA CAG AAG AGA GGA GC-3', Reverse 5'-CCT CTT TGC CAG AAG TTG AGA C-3'; PCSK6: Forward 5'-GAC TGG CTA AGC AGG CTT TCG A-3', Reverse 5'-TGC TGT TGG TGT AGC CAT CG CA-3'; EGFR: Forward 5'-AAC ACC CTG GTC TGG AAG TAC G-3', Reverse 5'-TCG TGG ACA GCC TTC AAG ACC-3'; GAPDH: Forward 5'-GTC TCC TCT GAC TTC AAC AGC G-3', Reverse 5'-ACC ACC CTG TTG CTG TAG CCA A-3'; miR-876-5p: 5'-GCC GAG TGG ATT TCT TTG T-3'; U6: 5'-GCC GAG TTC GGC AGC ACA TAT A-3'; Universal reverse primer: 5'-CTC AAC TGG TGT CGT GGA-3'.

Establishment of hsa_circ_103089 knockdown cell lines

Exons 12, 13, and 14 of the PCSK6 transcript make up hsa_circ_103089. To ensure specificity for hsa_circ_103089, shRNA sequences were manually designed to target the back-splice junction, preventing interference with the linear PCSK6 transcript. For recombinant production, the shRNAs were subsequently cloned into the pLKO.1 vector. Lentiviral packaging and purification were conducted by Zhejiang Ruyao Biotechnology Co., Ltd. Cell growth was sustained for five to seven days after the virus was introduced to A549 and HCC827 cells, supplemented with polybrene to improve infection and included 2 μg/ml puromycin for selection. After collecting cells, qRT-PCR was used to determine the silencing efficacy of hsa_circ_103089. The shRNA sequences were as follows: shRNA1: 5'-CCG GAC AGA AGA GAG GAG CAT CCC CCT CGA GGG GGA TGC TCC TCT CTT CTG TTT TTT G-3', 5'-AAT TCA AAA AAC AGA AGA GAG GAG CAT CCC CCC TCG AGG GGG ATG CTC CTC TCT TCT GT-3'; shRNA2: 5'-CCG GAG AGA GAG GAG CAT CCC CTT CTC GAG AAG GGG ATG CTC CTC TCT TCT TTT TTT G-3', 5'-AAT TCA AAA AGA AGA GAG GAG CAT CCC TCT CGA GAA GGG GAT GCT CCT CTC TTC T-3'; shRNA3: 5'-CCG GAA GAG AGG AGC ATC CCC TTA GCT CGA GCT AAG GGG ATG CTC CTC TCT TTT TTT T-3', 5'-CCG GAA GAG AGG AGC ATC CCC TTA GCT CGA GCT AAG GGG ATG CTC CTC TCT TTT TTT T-3'.

Transwell assay

Add 800 μL of complete culture medium containing serum to the lower chamber of the Transwell chamber, and inoculate the cell suspension (2×10^4 cells/well) into the upper chamber (using 8 μm pore size, Corning). The upper chamber was evenly smeared with Matrigel glue to form a gel, and the cell suspension was added with a total volume of 200 μL. After 48 h, fix the cells on the surface of the lower chamber with 4% paraformaldehyde and stain with 1% crystal violet.

Wound-healing assay

Inoculate cells at an appropriate density into a 6-well plate, and when the cell confluence is 100%, use a 10 μL pipette tip to draw lines along a ruler. Observe and photograph the cells after marking them with a phase contrast microscope, denoted as 0 h. After 48 h, continue with the same operation. The transfer distance was quantified using Image Pro Plus 6.0 software.

Cisplatin (DDP) sensitivity analysis

A549 or HCC827 cells were treated with 5 μM DDP for 24 h to determine their chemical sensitivity. Changes in cell viability were then measured using the CCK-8 test kit (HY-K0301,

MedChemExpress, USA). The cells were planted at a low density of 1000 cells per well on a 6-well plate and grown for two weeks in media with or without 5 μM DDP in order to perform the colony formation test, which assesses the survival of single cells under DDP stress. Following methanol fixation (Sigma), the cells were stained using a 1% crystal violet solution (Sigma). Following rinsing, pictures of the cells in every well were taken, and the number of visible colonies was tallied.

Extracellular Acidification Rate (ECAR) measurement

The ECAR, an indicator of glycolytic activity, was tracked using the Agilent Seahorse XFe24 Analyser in real time in compliance with the manufacturer's guidelines. Cells were seeded into XF24 cell culture microplates and incubated overnight, followed by serum starvation for 24 h. The cells were then equilibrated with non-buffered media, and sequential injections were performed as follows: 10 mM glucose at minute 14, 1 μM oligomycin at minute 35, and 80 mM 2-deoxy-D-glucose (2-DG, Sigma) at minute 56. ECAR was recorded in real-time and expressed as mpH/min. The following glycolytic parameters were calculated from the stress test: Glycolysis is equal to the final rate of ECAR measured before glucose infusion minus the maximal rate of ECAR measured prior to oligomycin injection; Glycolytic capacity is equal to the final ECAR rate recorded before glucose injection minus the greatest ECAR rate recorded following oligomycin treatment; Glycolytic capacity minus glycolysis equals glycolysis reversal.

Glucose and lactate content assay

Cells (5×10^6) were collected and lysed to determine glucose and lactate levels using the BC2505 glucose assay kit and BC2235 lactate assay kit from Beijing Solarbio in compliance with the manufacturer's guidelines. Results were reported in μmol/mg protein units. The ratio of lactate to glucose was used to assess the proportion of glycolytic activity.

Western blotting

Collect cells (5×10^6) or tissues (100 mg). Add RIPA lysis buffer containing protease inhibitors to lyse and extract cell or tissue proteins. Heat the protein at 100°C for 5 min for denaturation treatment. After protein separation by SDS-PAGE gel electrophoresis, the protein is transferred to the PVDF membrane (Millipore, Germany). The membrane was blocked with 3% bovine serum albumin (BSA, Sigma) at room temperature for 2 h. Primary antibodies [GLUT1 (ab115730, Abcam, UK), LDHA (ab47010, Abcam, UK), pPKM2 (ARG51804, Arigobio, China), PKM2 (ab85555, Abcam, UK), HK2 (ab209847, Abcam, UK), EGFR (ab52894, Abcam, UK), p-EGFR (11220, Signalway Biotechnology, USA), p-ERK (ab201015, Abcam, UK), ERK (ab54230, Abcam, UK), Histone H3 (ab18521, Abcam, UK), and β-actin (ab8226, Abcam, UK)] were incubated at 4°C for 16 h. Goat anti-rabbit IgG-HRP secondary antibody (ab6721, Abcam, UK) was applied and incubated at room temperature for 1 hour. The blots were developed using an ECL chemiluminescent substrate and imaged with a ChemiDoc-It Imaging System W/BioChemi HR Camera. Results were quantified by densitometry using ImageJ software. All primary antibodies were purchased from Abcam.

FISH staining

Following the methodology outlined by Emmanuelle et al. [13], we conducted FISH experiments using the biological FISH detection kit (C10910, RiboBio, China) to perform the subcellular localization of hsa_circ_103089. The hsa_circ_103089 FISH probe, a multi-point oligonucleotide probe labeled with Cy3, was custom-synthesized by Zhejiang Ruyao Biotechnology Co., Ltd. After fixation with 4% paraformaldehyde, cells were permeabilized with PBS/0.5% Triton X-100. The FISH procedure was then performed according to the kit's instructions. The Cy3-labeled probe was hybridized with cells at 37°C in hybridization buffer (with an additional 20 U of RNase R added to 40 μL of buffer) overnight. Cells were incubated with DAPI for 5 min to counterstain the nucleus. Images were captured using a fluorescence microscope (DM500, Leica, Germany).

RNA pull-down assay

293T cells, at 50% confluence, were transfected with 50 nM of biotinylated miR-876-5p mimic using Lipofectamine 3000 (Invitrogen). Twenty-four hours post-transfection, cells were harvested and lysed in lysis buffer. The cell

lysates were incubated with pre-washed streptavidin magnetic beads (22307-1, Beaverbio, China) for 3 h. After washing the beads, RNA interacting with the miRNA was extracted using TRIzol reagent. The enrichment of hsa_circ_103089 was analyzed by qRT-PCR.

Dual-luciferase reporter assay

Based on the targeting binding sequences between hsa_circ_103089 and miR-876-5p, mutant sequences of hsa_circ_103089 were constructed. Similarly, mutant sequences of the EGFR 3'UTR were constructed according to the targeting binding sites. The pGL3-Basic vector created the dual luciferase reporter gene plasmids, with pRL-SV40 as the control plasmid. The recombinant plasmids for wild-type and mutant hsa_circ_103089 and wild-type and mutant EGFR were contracted to Zhejiang Ruyao Biotechnology for construction.

Construction of EGFR overexpression cells

Primers for overexpression of EGFR were designed based on its coding sequence available on NCBI (NCBI ID: NM_005228.5). Primer 1 had the following sequences: Forward: 5'-ttt aaa ctt aag ctt ggt acc GCA CTC TCA GTA CAA TCT GCT CTG A-3', and Reverse: 5'-tac tga gag tgc ACC ATA GGG GAT CGG GAG ATC-3'. Primer 2 comprised: Forward: 5'-cct atg gtG CAC TCT CAG TAC AAT CTG CTC TGA-3', and Reverse: 5'-ggt ttt aaa cgg gcc ctc tag aAC CAT AGG GGA TCG GGA GAT C-3'. Using A549 mRNA as a template, the EGFR sequence was successfully amplified by PCR employing the high-fidelity PrimeSTAR® GXL DNA Polymerase (Takara). The PCR-amplified fragment was cloned using the Vazyme ClonExpress Ultra One Step Cloning Kit V3 into the pCDNA 3.1 vector. A suitable number of cells were propagated to 50%-60% confluence at the time of transfection after being seeded in a 24-well plate. Transfection in A549 or HCC827 cells was performed using the X-tremeGENE™ HP DNA transfection reagent (Roche) with 5 μg of either pCDNA3.1-Negative Control or pCDNA3.1-EGFR and 100 nM of miR-876-5p mimic or inhibitor. The levels of gene or protein expression were analyzed 48 h after transfection.

TUNEL staining

We performed TUNEL staining using the TMR (Red) TUNEL Cell Apoptosis Detection Kit from Servicebio to assess the level of nuclear DNA damage. At 551 nm, the TMR was activated, and at 575 nm, it was released. A fluorescent microscope was used to record the experimental outcomes. Image-Pro Plus 6.0 (IPP 6.0) software was used to quantify and statistically analyze the TUNEL-positive rate.

Xenograft model

A549 cells with negative control (5×10^6) and those silenced for hsa_circ_103089 (5×10^6) were injected subcutaneously into the right axillary region of 6-week-old male nude mice weighing 21 ± 1 g. The animals were grouped as follows: 1. sh-NC group (A549 cells infected with sh-NC, n = 5); 2. sh-circ_103089 group (A549 cells with silenced hsa_circ_103089, n = 5); 3. sh-circ_103089 + antagomir group (A549 cells with silenced hsa_circ_103089, n = 5), and miR-876-5p antagomir (5 nmol per mouse) was injected into the tumor site every 2 days after tumor formation; 4. DDP + sh-NC group (A549 cells infected with sh-NC, n = 5), and DDP (2 mg/kg) was administered intraperitoneally every other day for 3 weeks; 5. DDP + sh-circ_103089 group (A549 cells with silenced hsa_circ_103089, n = 5) and DDP (2 mg/kg) were administered intraperitoneally every other day for 3 weeks. Tumor volume was measured every 5 days after inoculation. On day 25 after inoculation, the nude mice were euthanized using CO_2 euthanasia. Tumor tissues were harvested, fixed in 4% paraformaldehyde, embedded in paraffin, and sectioned for further analysis. Additionally, tumor protein lysates were prepared to evaluate the expression levels of p-EGFR, EGFR, p-ERK, and ERK using western blotting.

Pathological examination

After deparaffinization, tissue sections were placed in 0.01 M citrate buffer at pH = 6.0 and subjected to antigen retrieval in an autoclave at 121°C for 15 min. After that, the slices were treated for 20 min with 3% H_2O_2 to inhibit endogenous peroxidase activity. Non-specific binding was blocked with 1% BSA at room temperature for 20 min. Ki67 primary antibody (ab15580, Abcam, UK) was applied and incubated at 4°C for 16 h. After removal of the primary antibody, A secondary antibody from goat against rabbit IgG conjugated with FITC was utilized and incubated at room 3,3'-diami-

nobenzidine (DAB; Sigma). The sections were developed with DAB and counterstained with hematoxylin to visualize the cell nuclei. DNA damage levels in the tumor tissues were assessed using a TUNEL staining kit.

Statistical analysis

Data from the research are presented as the average ± standard deviation derived from three separate trials. A two-tailed Student's t-test was implemented to evaluate differences between the two groups. In cases where more than two groups were analyzed, an analysis of variance was conducted, supplemented by one-way ANOVA with Tukey's post hoc test. A *P*-value below 0.05 was deemed to signify statistically significant discrepancies. Statistical processing and data visualization were carried out using GraphPad Prism 8.0.

Results

High expression of hsa_circ_103089 correlates with poor prognosis in NSCLC patients

From the GEO database, differential expression data of circ_RNAs in NSCLC patients were obtained. Venn diagrams revealed that six circ_RNAs were significantly upregulated in both GSE158695 and GSE112214 patient detection datasets, with hsa_circ_103089 exhibiting the highest significance and the largest LogFC value, suggesting its potential importance in the occurrence and development of lung cancer (**Figure 1A**). The hsa_circ_103089 transcript is composed of exons 12/13 and 14 of the PCSK6 gene (NM_138324.3), with the circularization site formed by the tail-to-head connection of the 3' end of exon 12 and the 5' end of exon 14 (**Figure 1B**). To further refine the screening results from the GEO database, this study collected 30 NSCLC samples from our hospital to detect the differential expression levels of hsa_circ_103089 in cancerous and adjacent tissues. The results revealed a significant upregulation of hsa_circ_103089 expression in tumor samples (**Figure 1C**), consistent with the results of tissue FISH experiments (**Figure 1D**). Additionally, correlating the FISH experiment levels of hsa_circ_103089 with key clinical characteristics (**Table 1**) indicated that hsa_circ_103089 levels are associated with tumor size, survival, and TNM staging but show no significant difference concerning gender and age. Notably, patients with high levels of hsa_circ_103089 had a lower overall survival rate (**Figure 1E**), emphasizing its prognostic significance.

Silencing hsa_circ_103089 impairs lung cancer cell invasion and migration

Then, we selected the A549 and HCC827 cell lines, which endogenously express relatively high levels of hsa_circ_103089, for knockdown experiments (**Figure 2A**). The circular RNA hsa_circ_103089 demonstrated increased stability; treatment with the transcription inhibitor ActD significantly reduced the levels of the linear transcript gene PCSK6, whereas the decrease in hsa_circ_103089 was less pronounced compared to PCSK6 over a 6-24 hour period ($P < 0.05$, **Figure 2B**, **2C**). Two shRNA constructs, sh-circ_103089#1 and sh-circ_103089#3, showed a significant suppressive effect on hsa_circ_103089 expression (**Figure 2D**). Both constructs markedly reduced the invasion capacity of A549 and HCC827 cells (**Figure 2E**, **2F**) and their migratory distance within 48 h (**Figure 2G**, **2H**).

Silencing hsa_circ_103089 enhances sensitivity of NSCLC cells to DDP

The suppression of hsa_circ_103089 markedly decreased the survival rate of NSCLC cells as opposed to the control group (sh-NC) ($P < 0.05$). Moreover, the combined treatment of hsa_circ_103089 silencing and DDP markedly suppressed NSCLC cell viability, with statistically significant differences observed compared to the sh-NC + DDP group ($P < 0.01$, **Figure 3A**). Clonogenic assays confirmed that silencing hsa_circ_103089 significantly decreased the number of single-cell-derived colonies in A549 and HCC827 cells, inhibiting cellular survival ($P < 0.05$ compared to the sh-NC group). The combined treatment of hsa_circ_103089 silencing and DDP significantly potentiated the inhibitory effect of DDP on the clonogenic survival of NSCLC cells, with statistically significant differences compared to the sh-NC + DDP group ($P < 0.01$, **Figure 3B**, **3C**).

hsa_circ_103089 regulates glycolytic capacity in NSCLC cells

ECAR assay results indicated that sh-circ_103089#1 and sh-circ_103089#3 significant-

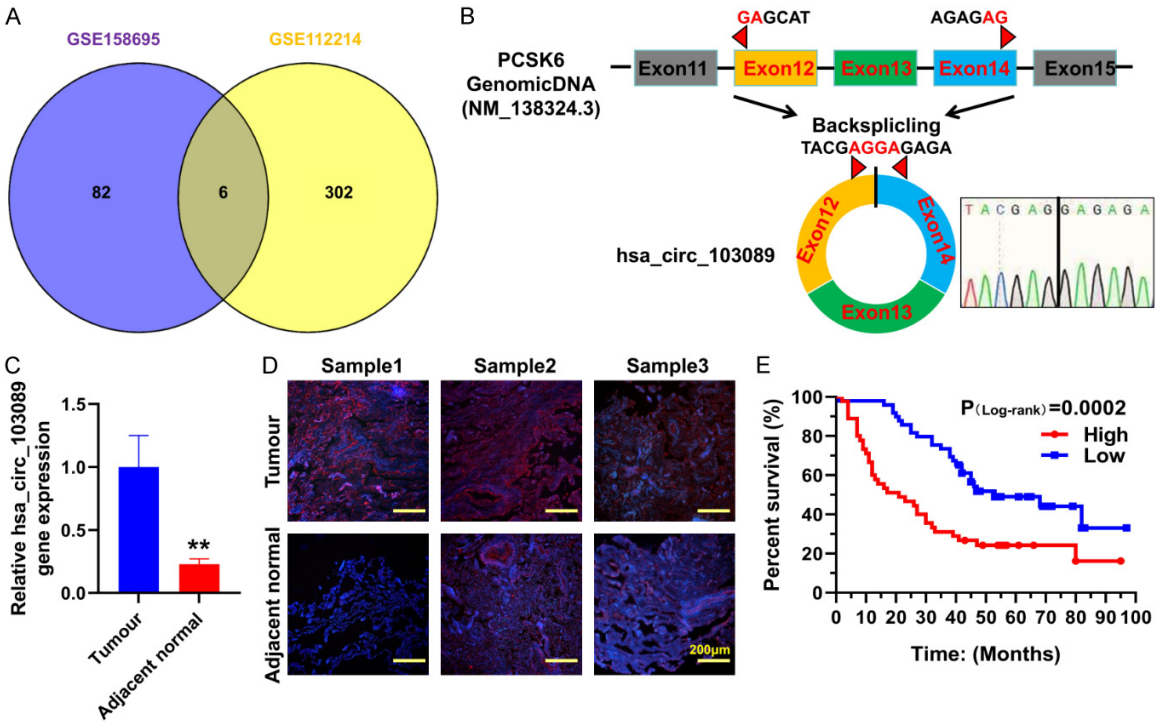

Figure 1. Analysis of the clinical correlation of hsa_circ_103089 with NSCLC patients. A. GEO database screening for significantly highly expressed circ_RNAs. B. Transcript information and circularization structure diagram of hsa_circ_103089. C. Expression levels of hsa_circ_103089 in cancerous and adjacent tissues of NSCLC patients. D. FISH experiment detecting the expression intensity of hsa_circ_103089 in cancerous and adjacent tissues of NSCLC patients (magnification, 100×). E. Prognosis analysis of hsa_circ_103089 expression intensity in NSCLC patients. $^{**}P < 0.01$, indicating a statistically significant difference between groups. GEO, Gene Expression Omnibus; NSCLC, non-small cell lung cancer; FISH, Fluorescence in situ hybridization.

Table 1. Correlation between clinical characteristics and hsa_circ_103089 expression of patients with NSCLC

Clinical parameters	hsa_circ_103089		Chi-square	*P*_Value
	Low	High		
Age				
≥ 60	36	27	0.64	0.42
< 60	15	16		
Sex				
Male	26	26	0.85	0.36
Female	25	17		
Tumor size (cm)				
≥ 5	19	25	4.09	0.04*
< 5	32	18		
TNM stage				
I-II	36	14	13.55	< 0.01**
III	15	29		
Survival time (M)				
≥ 36	34	18	5.81	0.02*
< 36	17	25		

$^{*}P < 0.05$, $^{**}P < 0.01$, indicating a statistically significant difference. NSCLC, non-small cell lung cancer.

ly reduced the glycolytic capacity of A549 and HCC827 cells (**Figure 4A-D**), including decreased glucose uptake, glycolytic flux, and acid production, compared to the sh-NC group ($P < 0.01$). Under DDP stress, the uptake of glucose (**Figure 4E**) and the production of lactate (**Figure 4F**) in A549 and HCC827 cells were significantly inhibited. Concurrently, the lactate-to-glucose uptake ratio (**Figure 4G**) also significantly decreased, exhibiting statistically significant disparities from the sh-NC group ($P < 0.05$). The sh-circ_103089#3 construct significantly amplified the suppressive impact of DDP on glucose absorption, lactate production, and the lactate-to-glucose ratio in NSCLC cells, with statistically significant differences compared to the sh-NC + DDP group ($P < 0.01$). Further examination of glycolysis-related proteins by Western blotting revealed that sh-circ_103089#3 notably

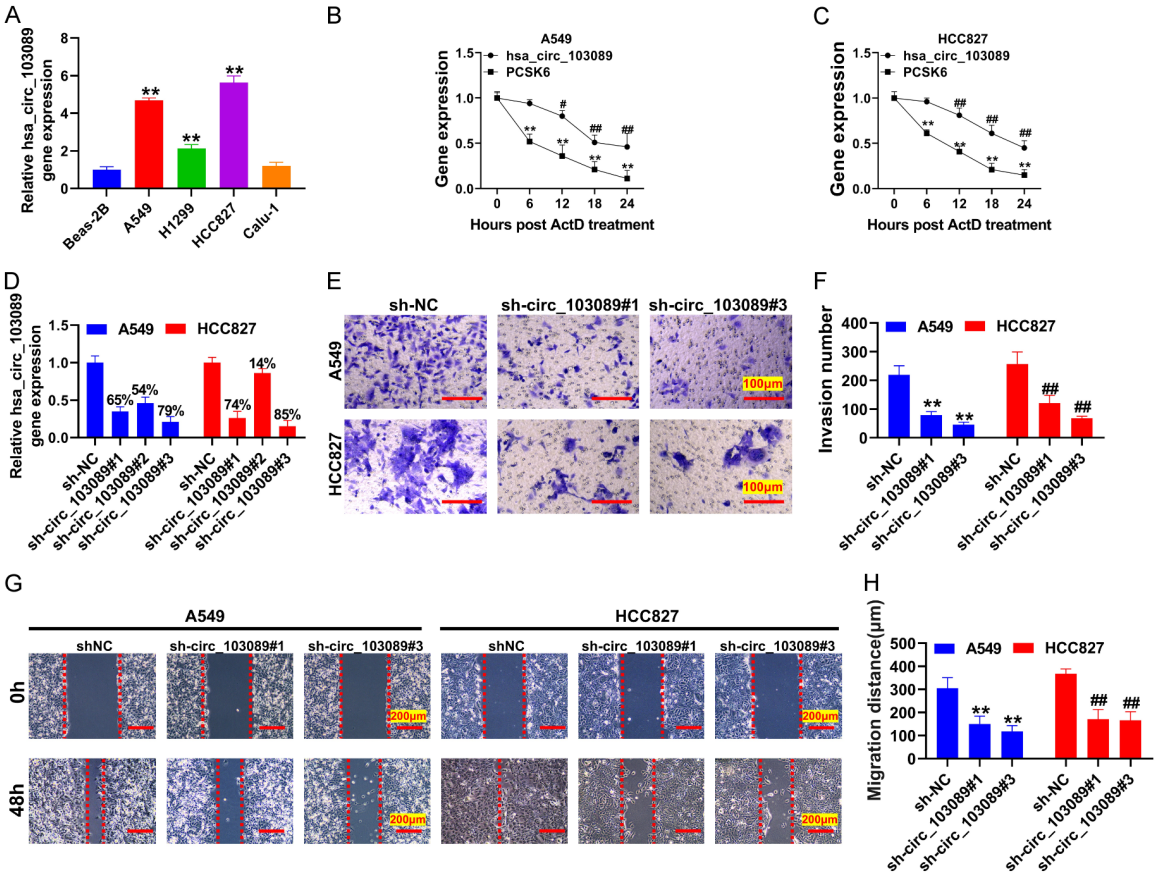

Figure 2. Silencing hsa_circ_103089 impairs the invasive and migratory capacities of lung cancer cells. A. qRT-PCR analysis of hsa_circ_103089 expression levels across various cell lines. B, C. Expression levels of hsa_circ_103089 and its linear transcript gene PCSK6 following treatment with the transcriptional inhibitor actinomycin D. D. Validation of shRNA-mediated silencing efficiency of hsa_circ_103089 by qRT-PCR. E, F. Transwell assays measure the number of invading cells (magnification, 400×). G, H. Wound-healing assays tracked cell migration distance over 48 h (magnification, 100×). $^{**}P < 0.01$, compared to the Beas-2b or 0 h or A549 cell sh-NC group; for HCC827 cells, $^{\#\#}P < 0.01$, $^{\#}P < 0.05$, compared to the sh-NC group, indicating statistically significant differences. ActD, actinomycin D; NC, negative control.

intensified the inhibitory effects of DDP on the expression levels of HK2, LDHA, PKM2, and GLUT1 proteins. The differences between the sh-circ_103089#3 + DDP group and the sh-NC + DDP group were statistically significant ($P < 0.01$, **Figure 4H-L**). Given the potential link between hypoxia and metabolic reprogramming, we next examined whether hypoxic conditions influence the expression of hsa_circ_103089. After exposing A549 and HCC827 cells to 1% O_2 for 24 hours, FISH staining revealed a marked increase in hsa_circ_103089 expression under hypoxia (Figure S2).

Targeting of miR-876-5p by hsa_circ_103089

As a circular RNA, hsa_circ_103089's ability to adsorb miRNAs is a crucial pathway for its functional effects. FISH experiments revealed that hsa_circ_103089 is widely distributed within cells, including both the cytoplasm and nucleus, with a predominant nuclear localization (**Figure 5A**). To identify the key miRNA regulated by hsa_circ_103089 in NSCLC, we integrated data from the GEO database, which identified 24 miRNAs significantly downregulated in NSCLC patients (GSE29250) with a P value < 0.01 and LogFC < -1. By performing a Venn diagram analysis with the 8 predicted target miRNAs of hsa_circ_103089, miR-876-5p emerged as the sole target miRNA (**Figure 5B**). Both sh-circ_103089#1 and sh-circ_103089#3 significantly upregulated the expression levels of miR-876-5p in A549 and HCC827 cells, with sh-circ_103089#3 showing

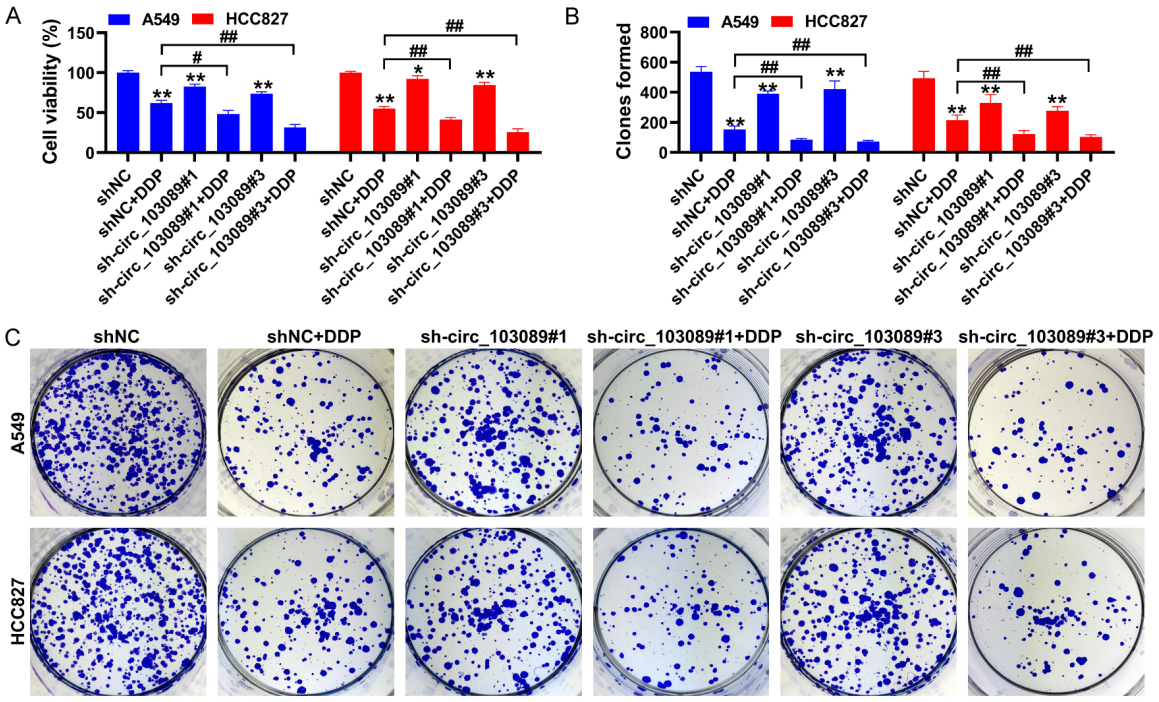

Figure 3. Silencing hsa_circ_103089 enhances sensitivity of NSCLC cells to DDP. A. CCK-8 assay evaluating the impact of hsa_circ_103089 on the viability of NSCLC cells under DDP treatment. B, C. Clonogenic assays assessed the survival capacity of single cells under DDP stress. $^{**}P < 0.01$, $^{*}P < 0.05$ compared to the sh-NC group; $^{\#\#}P < 0.01$, $^{\#}P < 0.05$ compared to the sh-NC + DDP group, indicating statistically significant differences. DDP, cisplatin; NSCLC, non-small cell lung cancer; NC, negative control.

the most pronounced effect ($P < 0.01$ compared to the sh-NC group, **Figure 5C**). A mutant type of hsa_circ_103089 was constructed based on the targeting binding sites with miR-876-5p (**Figure 5D**). Dual luciferase reporter assays confirmed that miR-876-5p mimic significantly reduced the relative fluorescence expression of the wild-type hsa_circ_103089 plasmid ($P < 0.01$), but did not affect the mutated hsa_circ_103089 plasmid's fluorescence expression (**Figure 5E**). A biotin magnetic bead probe linked to miR-876-5p was prepared, and RNA pull-down assays demonstrated that miR-876-5p binds to the hsa_circ_103089 transcript (**Figure 5F**), significantly upregulating the expression levels of hsa_circ_103089 compared to the input group ($P < 0.01$).

hsa_circ_103089 regulates the proliferative activity, migration, and invasion of NSCLC cells via miR-876-5p

To confirm the modulatory influence of hsa_circ_103089 on the migratory behavior (**Figure 6A-D**), invasion (**Figure 6E-G**), and proliferation (**Figure 6H**, **6I**) of NSCLC cells are mediated through its key target miR-876-5p, we conducted rescue experiments using miR-876-5p mimic and inhibitor. The findings demonstrated that sh-circ_103089#3 significantly reduced the migration distance and the number of invasive events. Cell viability of A549 and HCC827 cells was significantly enhanced after transfection with the mimic, with statistically significant differences between the sh-circ_103089#1/3 + mimic and sh-circ_103089#1/3 groups ($P < 0.05$). Conversely, The transfection with the inhibitor notably counteracted the suppressive effects of sh-circ_103089#3 on the migration distance, invasion count, and viability of A549 and HCC827 cells, with statistically significant differences observed when comparing the sh-circ_103089#3 + inhibitor group to the sh-circ_103089#3 group ($P < 0.05$).

hsa_circ_103089 regulates glycolytic capacity in NSCLC cells via miR-876-5p

The ECAR assay findings (**Figure 7A-D**) indicated that introducing miR-876-5p mimics into A549 and HCC827 cells significantly decreased glycolytic activity. This reduction in glycolytic

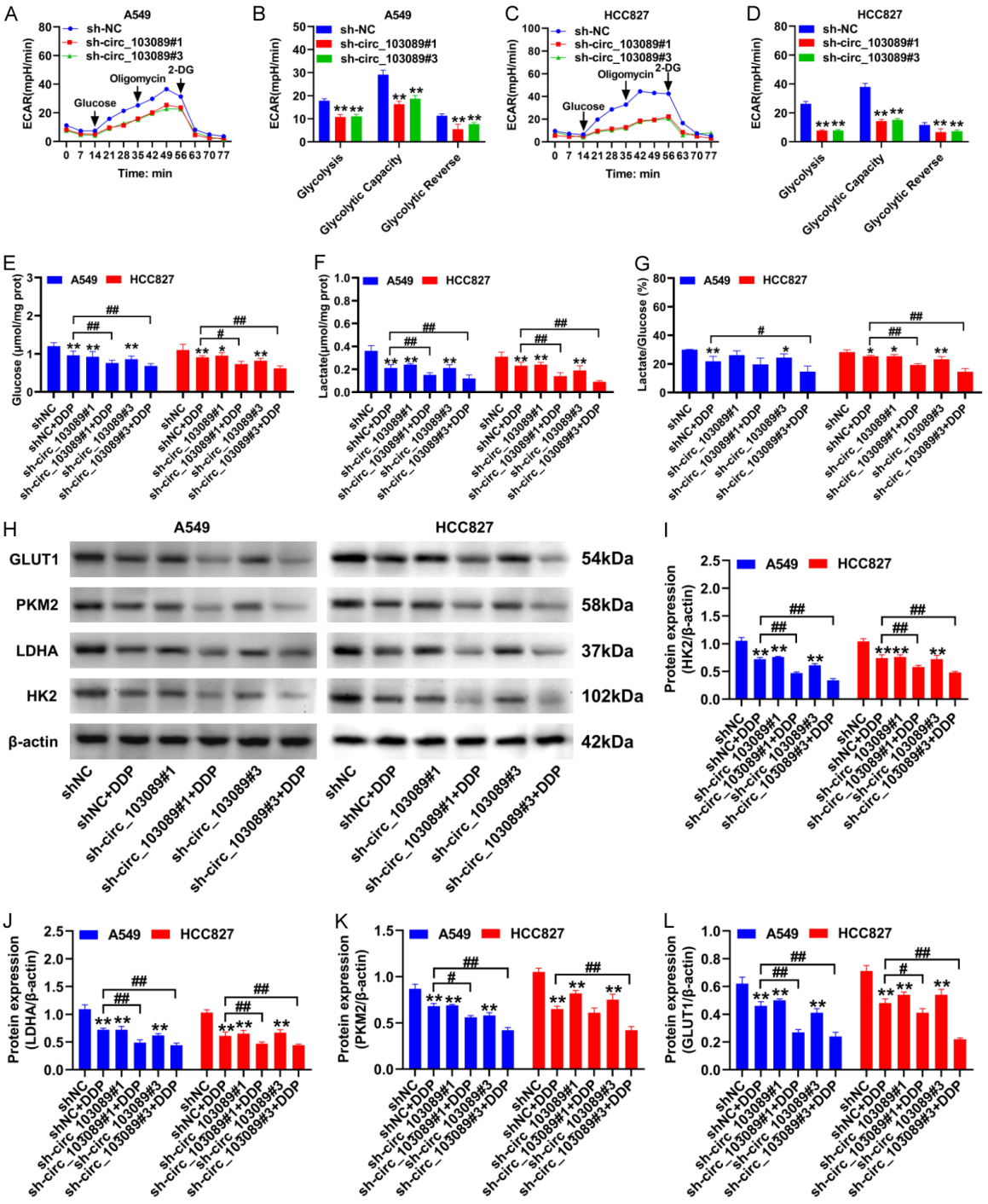

Figure 4. hsa_circ_103089 influences the glycolytic capacity of NSCLC cells. A-D. ECAR assays measure the ECAR to determine the glycolytic capacity of NSCLC cells in vitro, with ECAR values used to analyze specific differences in glycolytic activity levels. E. Detection of intracellular glucose content. F. Measurement of intracellular lactate content. G. Analysis of the lactate-to-glucose ratio to assess the preference for glycolytic pathways. H-L. Western blotting to detect the expression levels of glycolytic proteins HK2, LDHA, PKM2, and GLUT1, with quantification of band density values. $^{**}P < 0.01$, $^{*}P < 0.05$ compared to the sh-NC group; $\#\#P < 0.01$, $\#P < 0.05$ compared to the sh-NC + DDP group, indicating statistically significant differences. ECAR, Extracellular Acidification Rate; NSCLC, non-small cell lung cancer; DDP, cisplatin; NC, negative control.

capacity impaired the cells' ability to metabolize glucose and lowered their acid secretion rates. Statistically significant differences ($P < 0.01$) were observed when these results were

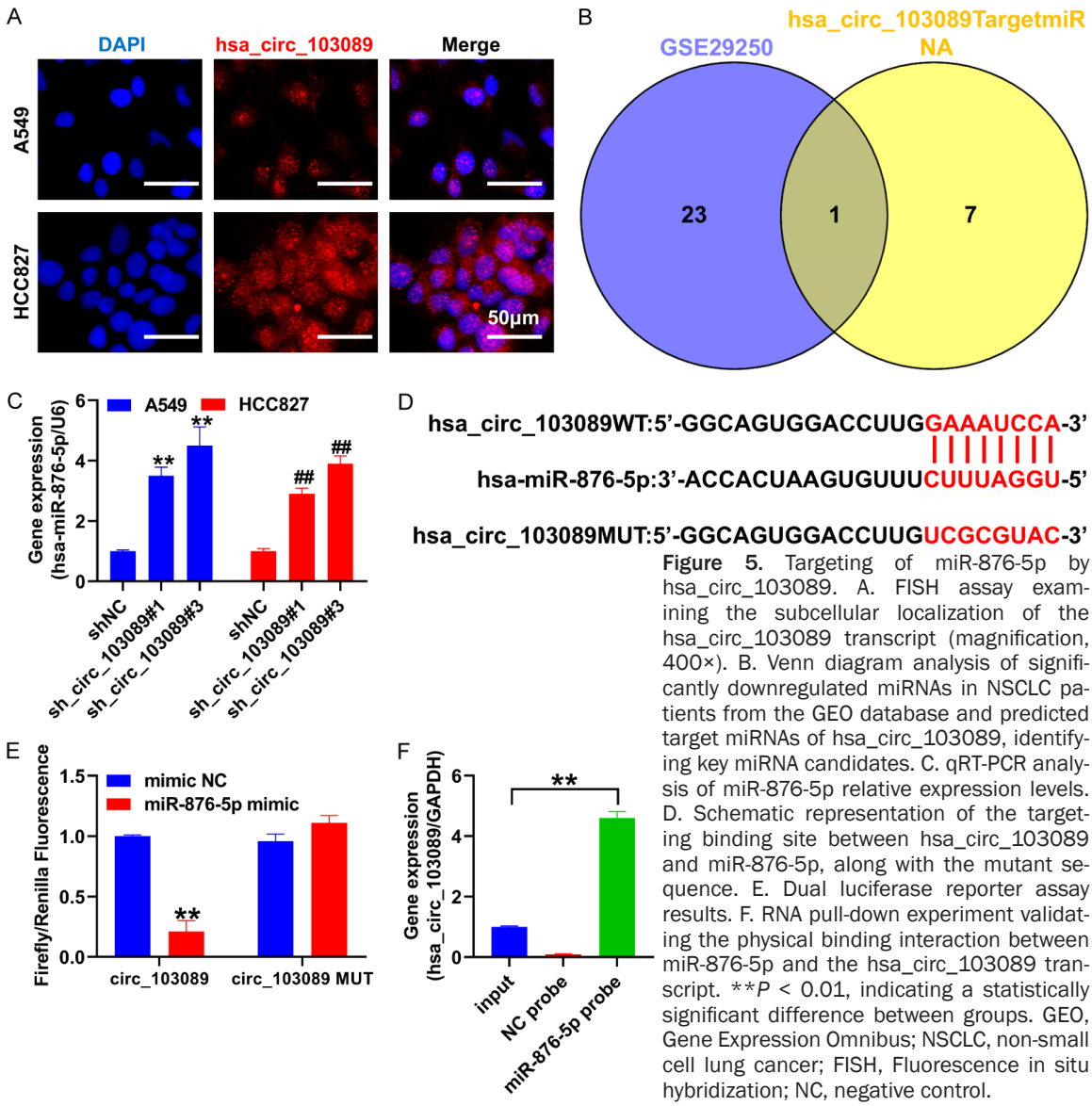

Figure 5. Targeting of miR-876-5p by hsa_circ_103089. A. FISH assay examining the subcellular localization of the hsa_circ_103089 transcript (magnification, 400×). B. Venn diagram analysis of significantly downregulated miRNAs in NSCLC patients from the GEO database and predicted target miRNAs of hsa_circ_103089, identifying key miRNA candidates. C. qRT-PCR analysis of miR-876-5p relative expression levels. D. Schematic representation of the targeting binding site between hsa_circ_103089 and miR-876-5p, along with the mutant sequence. E. Dual luciferase reporter assay results. F. RNA pull-down experiment validating the physical binding interaction between miR-876-5p and the hsa_circ_103089 transcript. $^{**}P < 0.01$, indicating a statistically significant difference between groups. GEO, Gene Expression Omnibus; NSCLC, non-small cell lung cancer; FISH, Fluorescence in situ hybridization; NC, negative control.

compared to the control groups of A549 or HCC827 cells. On the contrary, the introduction of miR-876-5p inhibitors into NSCLC cells resulted in a significant enhancement of glycolytic activity, increased glycolytic potential post-glucose uptake, and raised acid production levels. These changes were also statistically significant compared to the A549 or HCC827 control groups ($P < 0.01$). Western blot analysis of key glycolytic proteins (**Figure 7E-I**) further revealed that the miR-876-5p inhibitor notably reversed the suppressive effects of sh-circ_103089#1/3 on the expression of HK2, PKM2, LDHA, and GLUT1 in NSCLC cells. These reversals were statistically significant when contrasted with the sh-circ_103089#1 or 3 groups ($P < 0.01$).

miR-876-5p targets and regulates EGFR expression

We retrieved data on mRNAs significantly upregulated in NSCLC from the GEO database. We combined this with ENCORI data to predict miR-876-5p target mRNAs and GeneCard data on genes related to glycolysis. Venn diagram analysis (**Figure 8A**) indicated that EGFR and LDHA genes were significantly upregulated in NSCLC and are target mRNAs of miR-876-5p. EGFR has been shown in various cancer studies to regulate the expression of glycolytic proteins such as LDHA, PKM2, and HK2 [14-16]. Given that EGFR can exert a higher and more coordinated regulatory effect on glycolytic pathways, we focused more on its regulatory

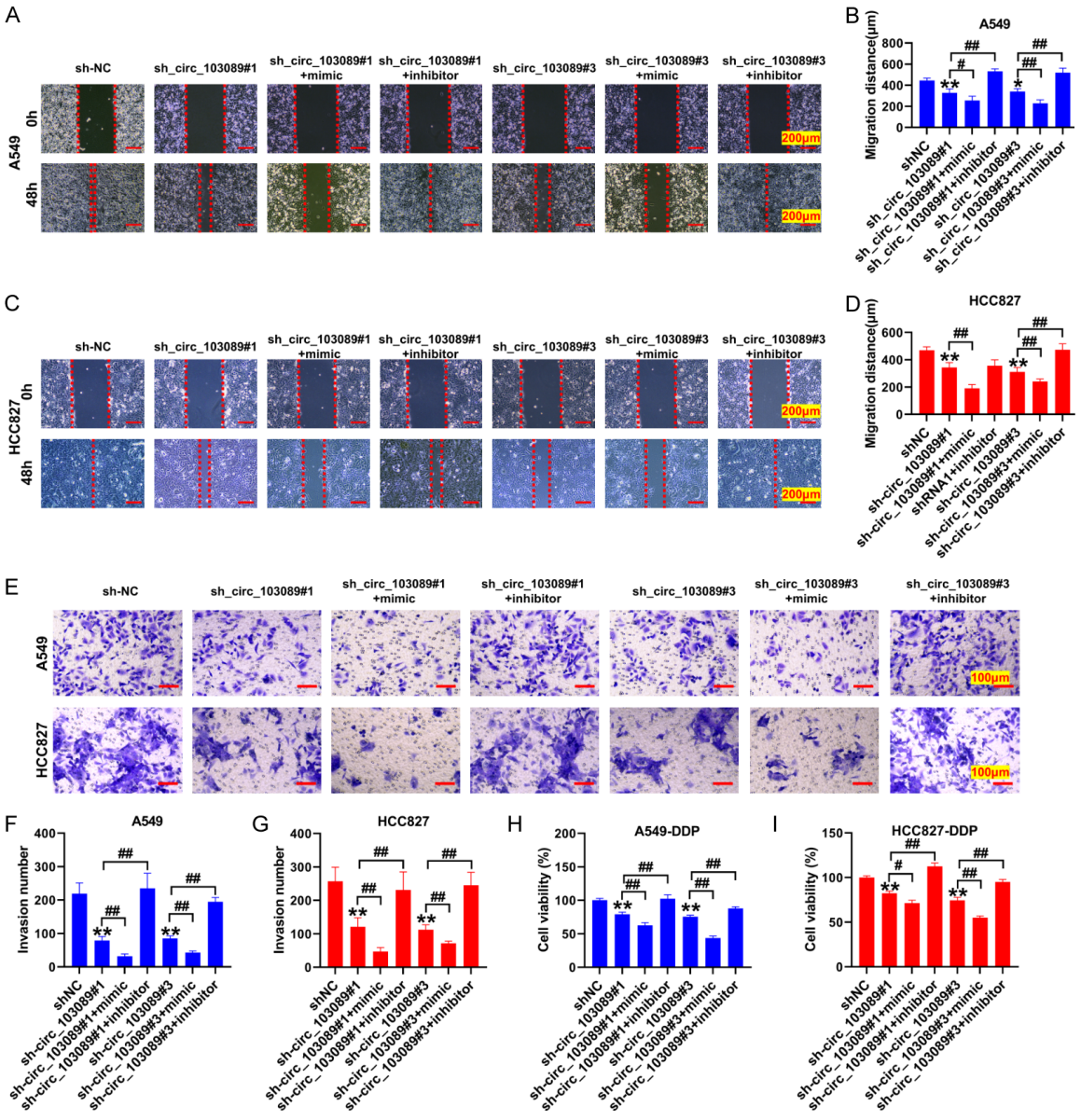

Figure 6. hsa_circ_103089 regulates the proliferative activity, migration, and invasion of NSCLC cells via miR-876-5p. A-D. Wound-healing assays measuring cell migration capacity (magnification, 100×). E-G. Transwell assays determine cell invasion numbers (magnification, 400×). H, I. CCK-8 assays assessing cell viability levels. $^{**}P < 0.01$, $^{*}P < 0.05$ compared to the sh-NC group; $\#\#P < 0.01$, $\#P < 0.05$ indicating statistically significant differences between groups. NC, negative control; CCK-8, Cell Counting Kit-8.

role. Under the action of shRNA, the expression of the EGFR gene was significantly downregulated, while the inhibitor notably reversed the suppressive effect of hsa_circ_103089 shRNA on EGFR gene expression levels ($P < 0.01$, **Figure 8B**). A mutant EGFR plasmid was constructed based on the targeting binding sites with miR-876-5p (**Figure 8C**). Dual luciferase reporter assays demonstrated that the miR-876-5p mimic markedly decreased the relative luminescence of the wild-type EGFR construct ($P < 0.01$). At the same time, it had no significant impact on the luminescence of the mutated EGFR construct (**Figure 8D**). A construct overexpressing EGFR was established, and in this overexpression group (OE-EGFR), the expression of the EGFR gene in A549 and HCC827 cells was significantly higher than in the control overexpression group (OE-NC) ($P < 0.01$, **Figure 8E**). In NSCLC cells, the transfec-

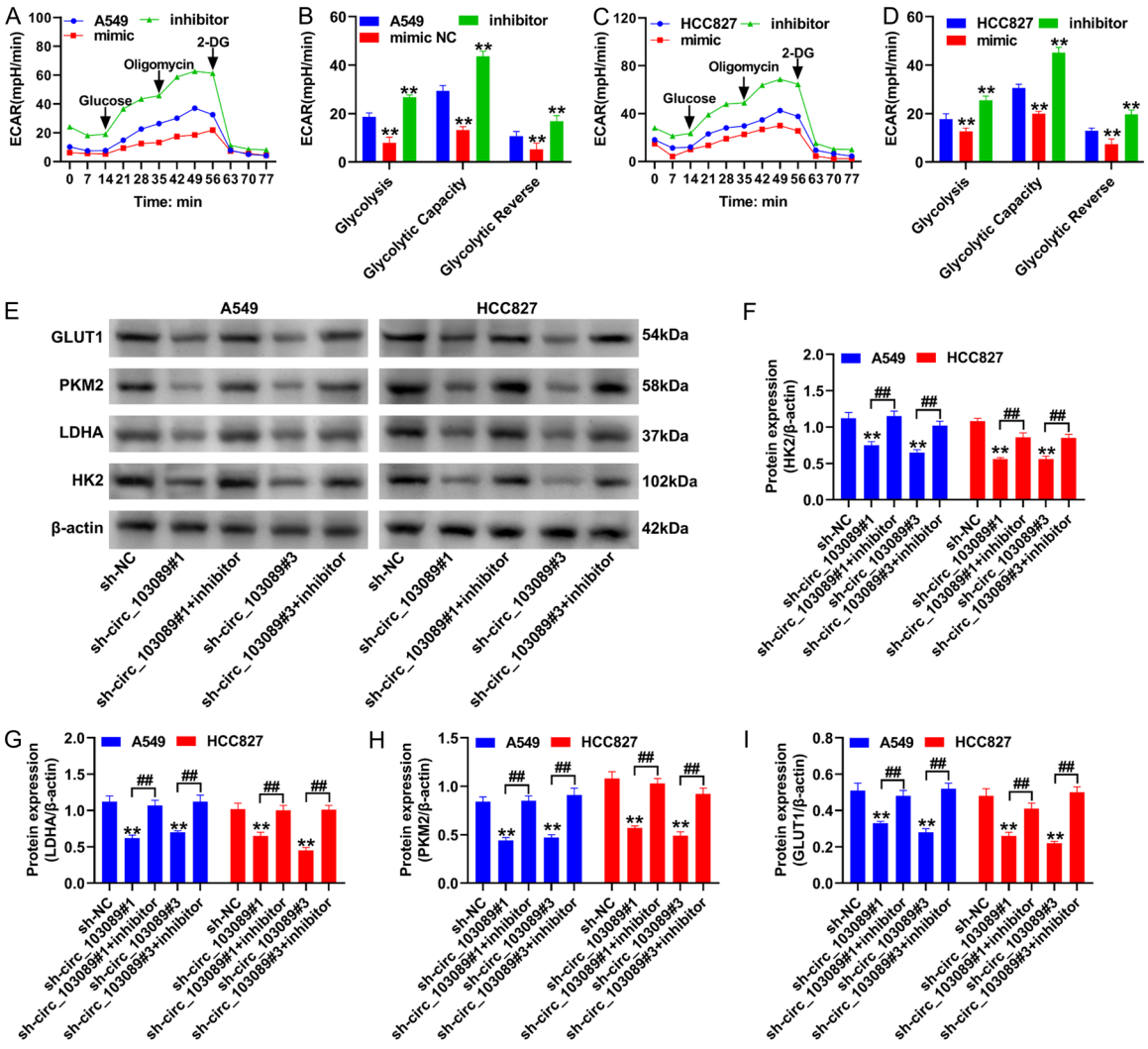

Figure 7. hsa_circ_103089 regulates the glycolytic capacity of NSCLC cells via miR-876-5p. A-D. ECAR assays measuring the ECAR to assess the glycolytic capacity of NSCLC cells in vitro, with calculated ECAR values used to analyze specific differences in glycolytic activity levels. E-I. Western blotting to detect glycolytic proteins HK2, LDHA, PKM2, and GLUT1 expression levels, including quantifying band density values. $^{**}P < 0.01$, $^{*}P < 0.05$ compared to the sh-NC group; $^{\#\#}P < 0.01$, $^{\#}P < 0.05$ indicating statistically significant differences between groups. ECAR, Extracellular Acidification Rate; NSCLC, non-small cell lung cancer; NC, negative control.

tion of miR-876-5p mimic or the knockdown of hsa_circ_103089 significantly mitigated the suppressive effects on phosphorylated EGFR and total protein levels induced by EGFR overexpression, with statistically significant differences when compared to the OE-EGFR group ($P < 0.01$, **Figure 8F-H**).

hsa_circ_103089 affects glycolytic gene and protein expression via the miR-876-5p/EGFR axis

qRT-PCR data revealed that the forced expression of EGFR led to a significant increase in the mRNA levels of LDHA, GLUT1, and HK2 genes ($P < 0.01$ versus the OE-NC group), while it had no significant influence on PKM2 gene expression ($P > 0.05$). The introduction of miR-876-5p mimics or the knockdown of hsa_circ_103089 in A549 and HCC827 cells notably counteracted the EGFR-induced upregulation of LDHA, GLUT1 and HK2 genes ($P < 0.01$ versus the EGFR group, **Figure 9A-D**). At the protein level, EGFR overexpression markedly elevated the phosphorylation levels of ERK1/2 and PKM2, exhibiting statistically significant differences compared to the OE-NC group ($P < 0.01$, **Figure**

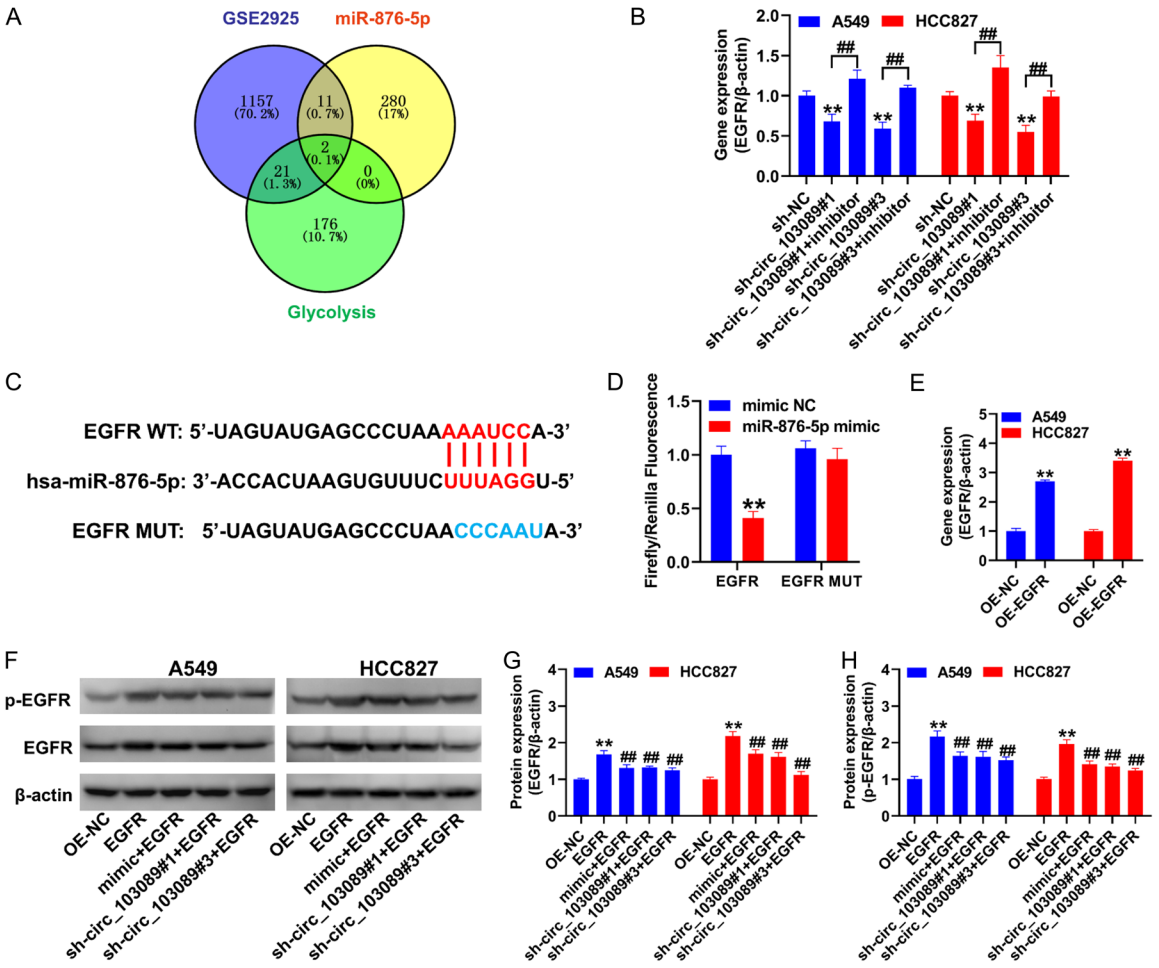

Figure 8. miR-876-5p targets and regulates EGFR expression. A. Analysis of mRNAs significantly upregulated in NSCLC patients obtained from the GEO database and prediction of miR-876-5p target mRNAs from the ENCORI database, with Venn diagram analysis identifying common target mRNAs among the three databases. B. qRT-PCR analysis of EGFR gene relative expression levels. C. Schematic representation of the targeting binding site between EGFR and miR-876-5p, along with the mutant sequence. D. Dual luciferase activity assay results. E. qRT-PCR detection of EGFR gene overexpression. F-H. Western blotting to detect the expression levels of EGFR and its phosphorylated protein. $^{**}P < 0.01$ compared to the sh-NC or OE-NC group; $^{\#\#}P < 0.01$ for group comparisons or compared to the EGFR group, indicating statistically significant differences. GEO, Gene Expression Omnibus; NSCLC, non-small cell lung cancer; ENCORI, The Encyclopedia of RNA Interactomes; NC, negative control.

9E-G). Additionally, EGFR overexpression enhanced the nuclear accumulation of PKM2 protein ($P < 0.01$). Conversely, the transfection of miR-876-5p mimics or the silencing of hsa_circ_103089 significantly mitigated the EGFR-mediated increase in ERK1/2 and PKM2 phosphorylation, as well as the nuclear translocation of PKM2 protein, with statistically significant differences compared to the EGFR group ($P < 0.05$, **Figure 9H**, **9I**).

hsa_circ_103089 regulates DDP sensitivity in NSCLC cells via the miR-876-5p/EGFR axis

DDP is known to induce DNA damage within the cell nucleus. To elucidate the role of hsa_circ_103089 in modulating the sensitivity of NSCLC to DDP via the miR-876-5p/EGFR pathway, we employed TUNEL staining to quantify nuclear DNA damage. Our findings indicated that EGFR overexpression in A549 and HCC827 cells significantly reduced the DDP-induced increase in TUNEL-positive cells, with a statistically significant difference observed between the EGFR and OE-NC groups ($P < 0.01$). The introduction of miR-876-5p mimics or the knockdown of hsa_circ_103089 notably reversed the EGFR overexpression-mediated decrease in TUNEL positivity ($P < 0.05$ compared to the EGFR group, **Figure 10A**, **10B**). Furthermore, CCK-8 assays assessing cell viability revealed

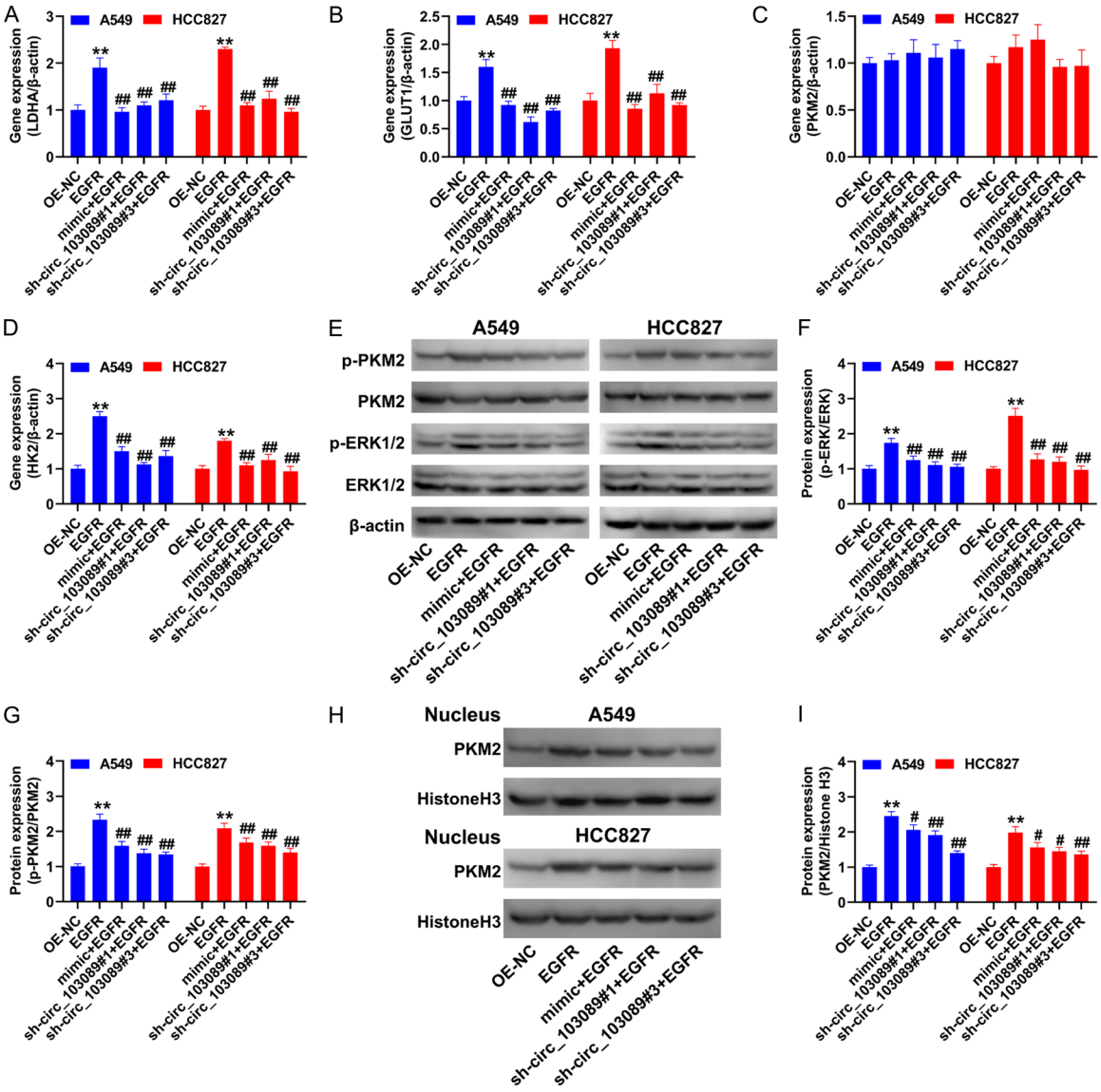

Figure 9. hsa_circ_103089 regulates glycolytic gene and protein expression via the miR-876-5p/EGFR axis. A-D. qRT-PCR analysis of LDHA, GLUT1, PKM2, and HK2 gene expression levels. E-G. Western blotting detection of ERK1/2 and PKM2 protein phosphorylation levels. H, I. Western blotting detection of nuclear PKM2 protein expression levels. $^{**}P < 0.01$ compared to the OE-NC group; $^{\#\#}P < 0.01$ compared to the EGFR group, indicating statistically significant differences. NC, negative control.

that the transfection of miR-876-5p mimics or the silencing of hsa_circ_103089 significantly counteracted the EGFR overexpression-induced reduction in activity inhibition rates under DDP treatment ($P < 0.05$ compared to the EGFR group, **Figure 10C**).

hsa_circ_103089 regulates tumor sensitivity to DDP in lung cancer-bearing nude mice through miR-876-5p

To delve deeper into the impact of hsa_circ_103089 on the progression of lung cancer and its response to chemotherapy, we developed a nude mouse model of lung cancer by subcutaneous injection of lung cancer cells. Observations of tumor growth demonstrated that the knockdown of hsa_circ_103089 significantly inhibited tumor growth compared to the control group ($P < 0.01$), and this inhibitory effect was notably reversed by the administration of antagomiR-876-5p ($P < 0.05$). Moreover, the knockdown of hsa_circ_103089 significantly potentiated the tumor growth inhibitory effects of cisplatin (DDP) ($P < 0.01$) (**Figure**

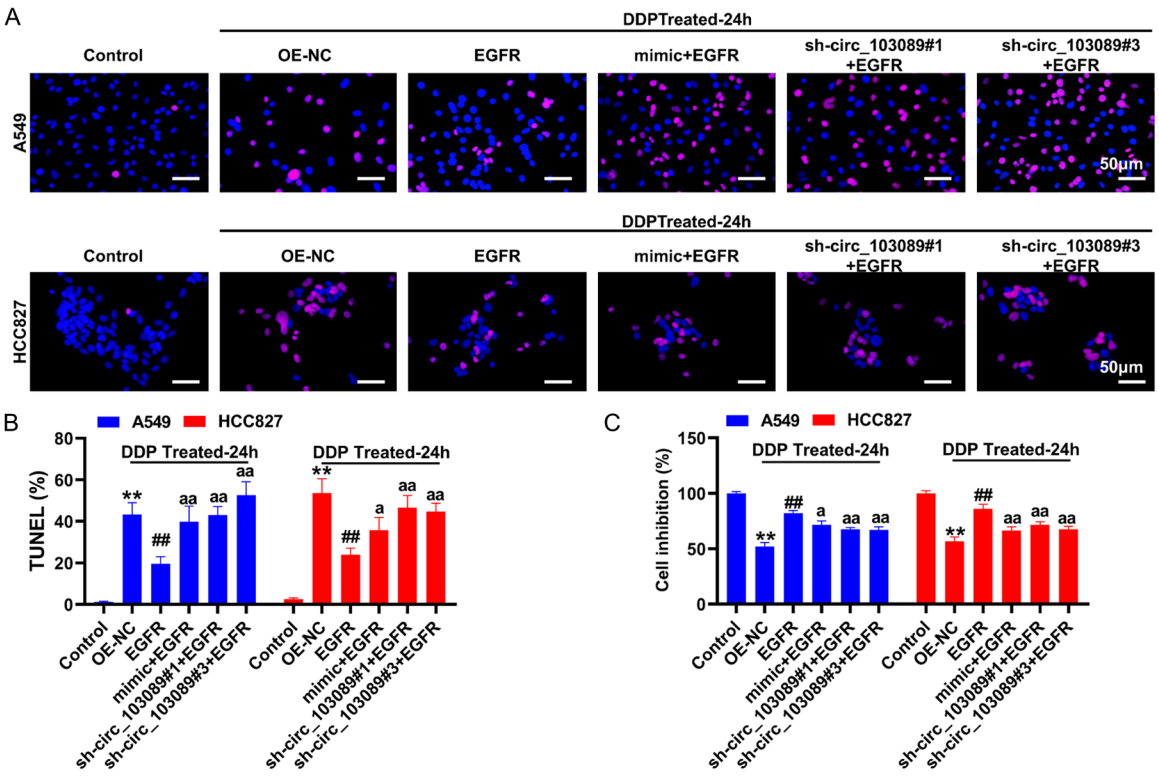

Figure 10. hsa_circ_103089 regulates sensitivity of NSCLC cells to DDP via the miR-876-5p/EGFR axis. A, B. TUNEL staining results, with TUNEL-positive cells indicated in red (magnification, 400×); C. CCK-8 assay evaluating the effect of different treatments on the inhibition rate of cells under DDP stress. $^{**}P < 0.01$ compared to the Control group; $^{\#\#}P < 0.01$ compared to the OE-NC group; $^{aa}P < 0.01$, $^{a}P < 0.05$ compared to the EGFR group, indicating statistically significant differences. DDP, cisplatin; CCK-8, cell counting Kit-8.

11A, **11B**). Ki67 immunodetection (**Figure 11C**) revealed that antagomiR-876-5p significantly counteracted the suppressive effect of hsa_circ_103089 knockdown on Ki67 expression ($P < 0.05$), and the knockdown of hsa_circ_103089 also significantly enhanced the inhibitory effect of DDP on Ki67 expression ($P < 0.01$). TUNEL staining (**Figure 11D**) indicated that the knockdown of hsa_circ_103089 significantly amplified the pro-apoptotic effect of DDP, as evidenced by increased TUNEL positivity (DDP + sh-circ_103089 group compared to DDP + sh-NC group, $P < 0.01$).

hsa_circ_103089 regulates glycolytic levels in lung cancer-bearing nude mice through miR-876-5p

qRT-PCR data (**Figure 12A-C**) revealed that the sh-circ_103089 group exhibited a significant reduction in hsa_circ_103089 expression levels ($P < 0.01$), whereas antagomiR-876-5p had no significant impact on hsa_circ_103089 expression ($P > 0.05$). Additionally, the knockdown of hsa_circ_103089 in DDP-treated cells significantly decreased hsa_circ_103089 expression levels ($P < 0.01$). AntagomiR-876-5p significantly counteracted the sh-circ_103089-induced upregulation of miR-876-5p ($P < 0.05$), and the knockdown of hsa_circ_103089 significantly increased miR-876-5p expression in tumors under DDP treatment ($P < 0.01$). In terms of EGFR gene expression, antagomiR-876-5p significantly reversed the sh-circ_103089-mediated downregulation of EGFR expression ($P < 0.05$), and the knockdown of hsa_circ_103089 also led to a significant decrease in EGFR expression in tumors under DDP treatment (DDP + sh-circ_103089 group compared to DDP + sh-NC group, $P < 0.01$).

Western blotting analyzes (**Figure 12D-F**) demonstrated that antagomiR-876-5p significantly counteracted the suppressive effect of sh-circ_103089 on the phosphorylation of EGFR and ERK1/2 proteins ($P < 0.05$). Additionally,

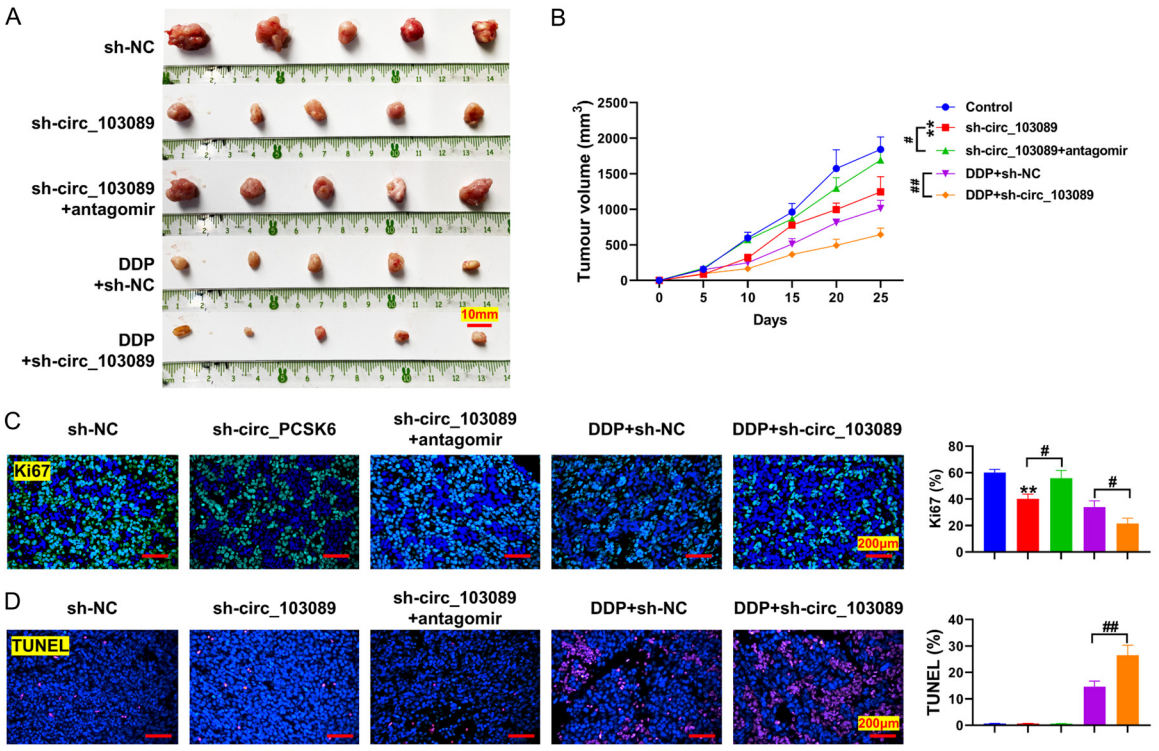

Figure 11. hsa_circ_103089 regulates tumor sensitivity to DDP and glycolytic levels in lung cancer-bearing nude mice through miR-876-5p. A. Tumor excision images; B. Tumor volume growth curves; C. Detection of Ki67 positivity in tumor tissues (magnification, 200×); D. Detection of TUNEL staining positivity in tumor tissues (magnification, 200×). $^{**}P < 0.01$ compared to the control group; $^{\#\#}P < 0.01$, $^{\#}P < 0.05$ indicating statistically significant differences between groups.

the knockdown of hsa_circ_103089 under DDP treatment significantly decreased the phosphorylation levels of EGFR and ERK1/2 proteins ($P < 0.01$). Moreover, antagomiR-876-5p significantly reversed the sh-circ_103089-mediated downregulation of glycolysis-associated proteins LDHA, HK2, PKM2, and GLUT1 ($P < 0.05$). The knockdown of hsa_circ_103089 also potentiated the inhibitory effect of DDP on the expression of LDHA, HK2, PKM2, and GLUT1 proteins (DDP + sh-circ_103089 group versus DDP + sh-NC group, $P < 0.01$) (**Figure 12G-J**).

Discussion

With the continuous advancement of lung cancer research, investigators have gradually recognized the pivotal regulatory role of circRNAs in human lung cancer. CircRNAs modulate a spectrum of processes, including differentiation, proliferation, migration, metastasis, and chemoresistance, through various mechanisms such as competitive endogenous RNA, transcriptional silencing complexes, and histone modifications. However, given the multitude of circRNAs and the diverse functional pathways they can influence, a profound understanding and expansion of knowledge regarding circRNAs with significant expression profiles are essential for elucidating the mechanisms underlying NSCLC and potentially impacting prognostic outcomes. This study showed a marked upregulation of hsa_circ_103089 in NSCLC tissues. Despite this, due to limited research, its role has not been documented in lung cancer or other cancers. Consequently, we researched the malignant characteristics of NSCLC, encompassing proliferation, invasion, migration, glycolysis, and sensitivity to DDP, to preliminarily elucidate the value of hsa_circ_103089 in NSCLC. Functional assays revealed that the silencing of hsa_circ_103089 significantly inhibits NSCLC cell proliferation, invasion, migration, and glycolysis while enhancing the sensitivity of NSCLC to DDP. Prior studies have confirmed that lung cancer cells' aberrant proliferation, invasion, migration, and even

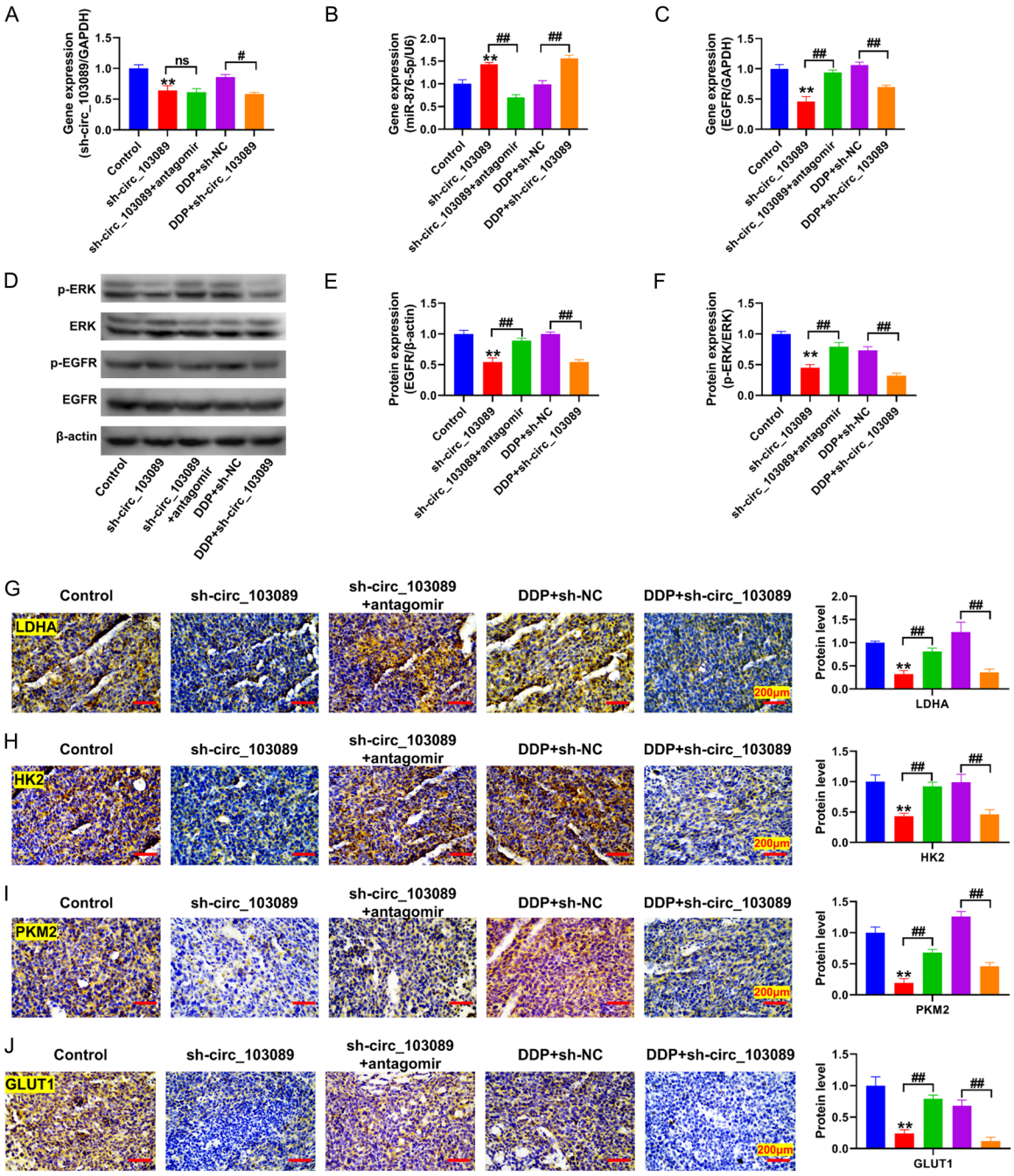

Figure 12. hsa_circ_103089 Regulates Glycolytic Levels in Lung Cancer-Bearing Nude Mice through miR-876-5p. A-C. qRT-PCR analysis of hsa_circ_103089, miR-876-5p, and EGFR gene expression levels in tumors; D-F. Western blotting detection of phosphorylated EGFR and ERK1/2 protein expression levels; G-J. Immunohistochemical analysis of glycolytic-related protein expression, including LDHA, HK2, PKM2, and GLUT1 (magnification, 200×). $^{**}P < 0.01$ compared to the control group; $^{\#\#}P < 0.01$, $^{\#}P < 0.05$ indicating statistically significant differences between groups.

DDP resistance can be regulated through the glycolytic pathway. Therefore, our subsequent research primarily focused on the mechanisms by which hsa_circ_103089 participates in the glycolytic pathway in NSCLC.

circRNAs, primarily derived from exons, are predominantly localized to the cytoplasm, serving as miRNA sponges. In contrast, circRNAs generated from introns are mainly nuclear and function as covalent binding elements [17].

Hsa_circ_103089, composed of three exons from the PCSK6 gene, was observed in our study to be expressed in both the cytoplasm and the nucleus. Given the maturity of research methodologies and the basis of previous experimental studies [18], we have elected to focus on the role of hsa_circ_103089 in regulating biological functions through its miRNA sponge activity.

circRNAs have been shown to function as competing endogenous RNAs (ceRNAs) to antagonize microRNAs (miRNAs), thereby modulating cancer progression. Evidence suggests that miRNAs act as oncogenes or tumor suppressor genes in various cancers, including NSCLC [19, 20]. In this context, we employed bioinformatics analysis to predict miRNAs associated with hsa_circ_103089 and demonstrated that miR-876-5p functions as a downstream miRNA of hsa_circ_103089 in NSCLC. Zhao et al. [21] have previously established that miR-876-5p can restrict the invasive capabilities of NSCLC by inhibiting the Wnt/β-catenin pathway. In this study, the researchers also observed the suppressive effects of miR-876-5p on invasion and migration. Moreover, miR-876-5p has been identified as an antitumor factor in endometrial cancer, where it suppresses the hexokinase domain containing 1 (HKDC1), thereby reducing lactate production and glycolytic capacity and exerting tumor-suppressive effects [22]. These findings provide our study's experimental basis and rationale, demonstrating that hsa_circ_103089 regulates glycolysis and subsequent malignant biological functions through miR-876-5p. Notably, using miRNA mimics and inhibitors, we have, for the first time, shown that miR-876-5p can enhance the sensitivity of NSCLC to DDP. This discovery further expands the potential functional impact of miR-876-5p in cancer research.

It is widely acknowledged that miRNA's most crucial and classic function is to regulate gene expression post-transcriptionally by targeting the 3'UTR of mRNA [23]. In this study, we utilized bioinformatics to predict the downstream targets of miR-876-5p, integrating data related to glycolysis and genes significantly upregulated in NSCLC from the GEO database. This preliminary analysis identified EGFR and LDHA as potential key targets of miR-876-5p. Reports indicate that EGFR plays a role in regulating glycolytic proteins such as HK2 [24], PKM2 [25], and GLUT1 [26]. By modulating EGFR, the glycolytic capacity of cancer cells can be notably reversed, leading to tumor suppression. Although miR-876-5p also exhibits regulatory effects on LDHA gene expression (Figure S1), its gene expression is concurrently influenced by EGFR levels, a phenomenon similarly observed in epithelial cells during pulmonary fibrosis [27]. Consequently, we posit that modulating EGFR could achievecomprehensive control over glycolytic function, making EGFR the primary downstream target for further investigation.

Currently, inhibitors targeting the epidermal growth factor receptor (EGFR) have become a standard therapeutic approach for NSCLC patients with EGFR-activating mutations. However, NSCLCs that overexpress EGFR without carrying these activating mutations tend to be resistant to EGFR inhibitors, and the mechanisms underlying this primary resistance to EGFR inhibitors in EGFR-activating mutation-negative NSCLCs remain largely elusive [28]. Research on non-mutated EGFR has shown that inhibiting EGFR can enhance the sensitivity of lung cancer cells to tyrosine kinase inhibitors, as demonstrated by Duan et al. [29], and higher levels of EGFR expression have been observed in DDP-resistant NSCLC cells [29]. Furthermore, the upregulation of factors activating the EGFR pathway can significantly promote the progression of NSCLC [30]. These findings underscore the importance of EGFR as a significant target in conventional lung cancer therapies.

Furthermore, we have noted that the PKM2 gene does not appear to be directly influenced by EGFR expression levels; however, its protein levels rise in tandem with the upregulation of EGFR protein expression. EGFR can enhance the phosphorylation of PKM2 protein at the S37 site by activating extracellular signal-regulated kinase (ERK1/2) proteins, thereby synergistically increasing the expression of LDHA and GLUT1 genes and proteins. Yang et al. have suggested that ERK phosphorylation-dependent nuclear translocation of PKM2 is essential for the self-regulation of PKM2 expression and PKM2-dependent glycolytic gene expression, which is vital for the Warburg effect promoted by EGFR and tumorigenesis [31]. Numerous studies have corroborated this phenomenon, including those within lung cancer research

[25, 32]. Our study's findings indicate that the overexpression of EGFR upregulates the nuclear expression levels of PKM2 protein in A549 and HCC827 cells, which is believed to be associated with increased phosphorylation levels of ERK and PKM2 S37 site proteins. However, the regulatory effects of EGFR on ERK1/2 are not confined to PKM2 and glycolytic pathway-related proteins; they can also directly influence lung cancer cells' proliferative, migratory, and invasive capabilities [33]. This insight directly elucidates why the hsa_circ_103089/miR-876-5p pathway can modulate cellular invasiveness and migratory abilities. Meanwhile, under hypoxic conditions, the expression of hsa_circ_103089 in A549 and HCC827 cells increased significantly (Figure S2), which may further promote cell proliferation.

This study has notable limitations: the lack of clinical sample data is the most significant shortfall, particularly concerning samples from patients with DDP-resistant NSCLC. Access to these samples is essential for clarifying the role of hsa_circ_103089 in patients with DDP resistance and understanding the poor progression of NSCLC, which would have considerable implications for clinical research. Moreover, based on the subcellular localization of hsa_circ_103089, our investigation has focused on its role in the cytoplasm, which modulates the miR-876-5p/EGFR axis. Its presence in the nucleus suggests that hsa_circ_103089 may have the capacity to bind with nucleic acids or even nuclear proteins covalently. A thorough elucidation of the functions of hsa_circ_103089 from various angles and directions could offer a more extensive theoretical and experimental foundation for explaining the pathogenesis and treatment options for NSCLC.

Conclusions

In this study, we first established the association of hsa_circ_103089 with the migration, invasion, glycolysis, and DDP sensitivity of NSCLC cells using bioinformatics and functional biological assays. Mechanistically, we demonstrated that hsa_circ_103089 can enhance the expression of the EGFR gene and protein by directly binding to miR-876-5p, increasing the phosphorylation levels of ERK1/2 and PKM2 proteins. The phosphorylated PKM2 then translocates to the nucleus, promoting the coordinated expression of glycolytic proteins such as LDHA, GLUT1, and HK2, thereby enhancing glycolytic function. Furthermore, hsa_circ_103089, through the miR-876-5p/EGFR axis, also diminishes the sensitivity of NSCLC to DDP. Consequently, the presence of hsa_circ_103089 could serve as a potential biomarker for predicting the malignant progression and chemotherapeutic response of NSCLC.

Acknowledgements

Thanks to Zhejiang Ruyao Biotechnology Co., Ltd. for their technical guidance in cell culture. This study was supported by the Medical Health Science and Technology Project of Zhejiang Provincial Health Commission (No. 2023KY275), the Natural Science Foundation of Zhejiang Province (No. LQ21H160014), the Ningbo Clinical Research Center for Respiratory Diseases (No. 2022L004), the Natural Science Foundation of Ningbo (No. 2023J318), and Key Research Foundation of Hwa Mei Hospital, University of Chinese Academy of Sciences (No. 2022HMZD09).

Disclosure of conflict of interest

None.

Address correspondence to: Zhaoxing Dong, Department of Respiratory and Critical Care Medicine, Ningbo No. 2 Hospital, 41 Northwest Street, Haishu District, Ningbo 315000, Zhejiang, China. E-mail: dongkm@hotmail.com

References

[1] GBD 2019 Respiratory Tract Cancers Collaborators. Global, regional, and national burden of respiratory tract cancers and associated risk factors from 1990 to 2019: a systematic analysis for the Global Burden of Disease Study 2019. Lancet Respir Med 2021; 9: 1030-1049.

[2] Xie S, Wu Z, Qi Y, Wu B and Zhu X. The metastasizing mechanisms of lung cancer: recent advances and therapeutic challenges. Biomed Pharmacother 2021; 138: 111450.

[3] Sheikhshabani SH, Modarres P, Ghafouri-Fard S, Amini-Farsani Z, Khodaee L, Shaygan N, Amini-Farsani Z and Omrani MD. Meta-analysis of microarray data to determine gene indicators involved in cisplatin resistance in non-small cell lung cancer. Cancer Rep (Hoboken) 2024; 7: e1970.

[4] Sun Y, Chen Y, Xu M, Liu C and Wang C. Shenmai injection supresses glycolysis and enhances cisplatin cytotoxicity in cisplatin-resistant A549/DDP cells via the AKT-mTOR-c-Myc signaling pathway. Biomed Res Int 2020; 2020: 9243681.
[5] Geng P, Zhao J, Li Q, Wang X, Qin W, Wang T, Shi X, Liu X, Chen J, Qiu H and Xu G. Z-ligustilide combined with cisplatin reduces PLPP1-mediated phospholipid synthesis to impair cisplatin resistance in lung cancer. Int J Mol Sci 2023; 24: 17046.
[6] Suzuki A, Puri S, Leland P, Puri A, Moudgil T, Fox BA, Puri RK and Joshi BH. Subcellular compartmentalization of PKM2 identifies anti-PKM2 therapy response in vitro and in vivo mouse model of human non-small-cell lung cancer. PLoS One 2019; 14: e0217131.
[7] Heiden MGV, Cantley LC and Thompson CB. Understanding the Warburg effect: the metabolic requirements of cell proliferation. Science 2009; 324: 1029-1033.
[8] Majem B, Nadal E and Muñoz-Pinedo C. Exploiting metabolic vulnerabilities of non small cell lung carcinoma. Semin Cell Dev Biol 2020; 98: 54-62.
[9] Wang S, Cheng Z, Cui Y, Xu S, Luan Q, Jing S, Du B, Li X and Li Y. PTPRH promotes the progression of non-small cell lung cancer via glycolysis mediated by the PI3K/AKT/mTOR signaling pathway. J Transl Med 2023; 21: 819.
[10] Kim JH, Nam B, Choi YJ, Kim SY, Lee JE, Sung KJ, Kim WS, Choi CM, Chang EJ, Koh JS, Song JS, Yoon S, Lee JC, Rho JK and Son J. Enhanced glycolysis supports cell survival in EGFR-mutant lung adenocarcinoma by inhibiting autophagy-mediated egfr degradation. Cancer Res 2018; 78: 4482-4496.
[11] Zhang L, Zhang Z and Yu Z. Identification of a novel glycolysis-related gene signature for predicting metastasis and survival in patients with lung adenocarcinoma. J Transl Med 2019; 17: 423.
[12] Guo F, Li S, Guo C, Xu X, Zhou X, Ma D, Cao Z, Bing Z and Cui Y. Circular RNA circMAGI3 accelerates the glycolysis of non-small cell lung cancer through miR-515-5p/HDGF. Am J Transl Res 2020; 12: 3953-3963.
[13] Querido E, Sfeir A and Chartrand P. Imaging of telomerase RNA by single-molecule inexpensive FISH combined with immunofluorescence. STAR Protoc 2020; 1: 100104.
[14] Song YD, Zhang KF, Liu D, Guo YQ, Wang DY, Cui MY, Li G, Sun YX, Shen JH, Li XG, Zhang L and Shi FJ. Inhibition of EGFR-induced glucose metabolism sensitizes chondrosarcoma cells to cisplatin. Tumour Biol 2014; 35: 7017-7024.
[15] Makinoshima H, Takita M, Matsumoto S, Yagishita A, Owada S, Esumi H and Tsuchihara K. Epidermal growth factor receptor (EGFR) signaling regulates global metabolic pathways in EGFR-mutated lung adenocarcinoma. J Biol Chem 2014; 289: 20813-23.
[16] Zhong Z and Zhong H. KIF22 promotes the proliferation and glycolysis of melanoma by activating EGFR/STAT3 signaling. Clinics (Sao Paulo) 2023; 78: 100307.
[17] Li X, Yang L and Chen LL. The biogenesis, functions, and challenges of circular RNAs. Mol Cell 2018; 71: 428-442.
[18] Yang Y, Tai W, Lu N, Li T, Liu Y, Wu W, Li Z, Pu L, Zhao X, Zhang T and Dong Z. lncRNA ZFAS1 promotes lung fibroblast-to-myofibroblast transition and ferroptosis via functioning as a ceRNA through miR-150-5p/SLC38A1 axis. Aging (Albany NY) 2020; 12: 9085-9102.
[19] Li S, Qiu C, Sun D, Yang S and Wang L. circNINL facilitates aerobic glycolysis, proliferation, invasion, and migration in lung cancer by sponging miR-3918 to mediate FGFR1 expression. Eur J Med Res 2024; 29: 67.
[20] Zhang Y, Ge P, Zhou D, Xing R and Bai L. Circular RNA FOXO3 accelerates glycolysis and improves cisplatin sensitivity in lung cancer cells via the miR543/Foxo3 axis. Oncol Lett 2021; 22: 839.
[21] Zhao Y, Dai Q, Fu X, Chen Q, Tang Y, Gao X and Zhou Q. CircVAPA exerts oncogenic property in non-small cell lung cancer by the miR-876-5p/WNT5A axis. J Gene Med 2021; 23: e3325.
[22] Guo J, Ye F, Xie W, Zhang X, Zeng R, Sheng W, Mi Y and Sheng X. The HOXC-AS2/miR-876-5p/HKDC1 axis regulates endometrial cancer progression in a high glucose-related tumor microenvironment. Cancer Sci 2022; 113: 2297-2310.
[23] Pu M, Chen J, Tao Z, Miao L, Qi X, Wang Y and Ren J. Regulatory network of miRNA on its target: coordination between transcriptional and post-transcriptional regulation of gene expression. Cell Mol Life Sci 2019; 76: 441-451.
[24] Liu YH, Wei XL, Hu GQ and Wang TX. Quinolone-indolone conjugate induces apoptosis by inhibiting the EGFR-STAT3-HK2 pathway in human cancer cells. Mol Med Report 2015; 12: 2749-56.
[25] Biyik-Sit R, Kruer T, Dougherty S, Bradley JA, Wilkey DW, Merchant ML, Trent JO and Clem BF. Nuclear pyruvate kinase M2 (PKM2) contributes to phosphoserine aminotransferase 1 (PSAT1)-mediated cell migration in EGFR-activated lung cancer cells. Cancers (Basel) 2021; 13: 3938.
[26] Wu Y, Wang Y, Yao H, Li H, Meng F, Li Q, Lin X and Liu L. MNX1-AS1, a c-Myc induced lncRNA, promotes the Warburg effect by regulating

PKM2 nuclear translocation. J Exp Clin Cancer Res 2022; 41: 337.
[27] Massip-Copiz MM, Valdivieso ÁG, Clauzure M, Mori C, Asensio C, Aguilar MÁ and Santa-Coloma TA. Epidermal growth factor receptor activity upregulates lactate dehydrogenase A expression, lactate dehydrogenase activity, and lactate secretion in cultured IB3-1 cystic fibrosis lung epithelial cells. Biochem Cell Biol 2021; 99: 476-487.
[28] Suzuki S, Okada M, Takeda H, Kuramoto K, Sanomachi T, Togashi K, Seino S, Yamamoto M, Yoshioka T and Kitanaka C. Involvement of GLUT1-mediated glucose transport and metabolism in gefitinib resistance of non-small-cell lung cancer cells. Oncotarget 2018; 9: 32667-32679.
[29] Duan Z. MS4A3 promotes the chemosensitivity of lung cancer via THAP1/EGFR pathways. Crit Rev Eukaryot Gene Expr 2024; 34: 1-11.
[30] Fu H, Gao H, Qi X, Zhao L, Wu D, Bai Y, Li H, Liu X, Hu J and Shao S. Aldolase A promotes proliferation and G(1)/S transition via the EGFR/MAPK pathway in non-small cell lung cancer. Cancer Commun (Lond) 2018; 38: 18.
[31] Yang W, Zheng Y, Xia Y, Ji H, Chen X, Guo F, Lyssiotis CA, Aldape K, Cantley LC and Lu Z. ERK1/2-dependent phosphorylation and nuclear translocation of PKM2 promotes the Warburg effect. Nat Cell Biol 2012; 14: 1295-304.
[32] Yawut N, Kaowinn S, Cho IR, Budluang P, Kim S, Kim S, Youn SE, Koh SS and Chung YH. Translocalization of enhanced PKM2 protein into the nucleus induced by cancer upregulated gene 2 confers cancer stem cell-like phenotypes. BMB Rep 2022; 55: 98-103.
[33] Du R, Shen W, Liu Y, Gao W, Zhou W, Li J, Zhao S, Chen C, Chen Y, Liu Y, Sun P, Xiang R, Shi Y and Luo Y. TGIF2 promotes the progression of lung adenocarcinoma by bridging EGFR/RAS/ERK signaling to cancer cell stemness. Signal Transduct Target Ther 2019; 4: 60.

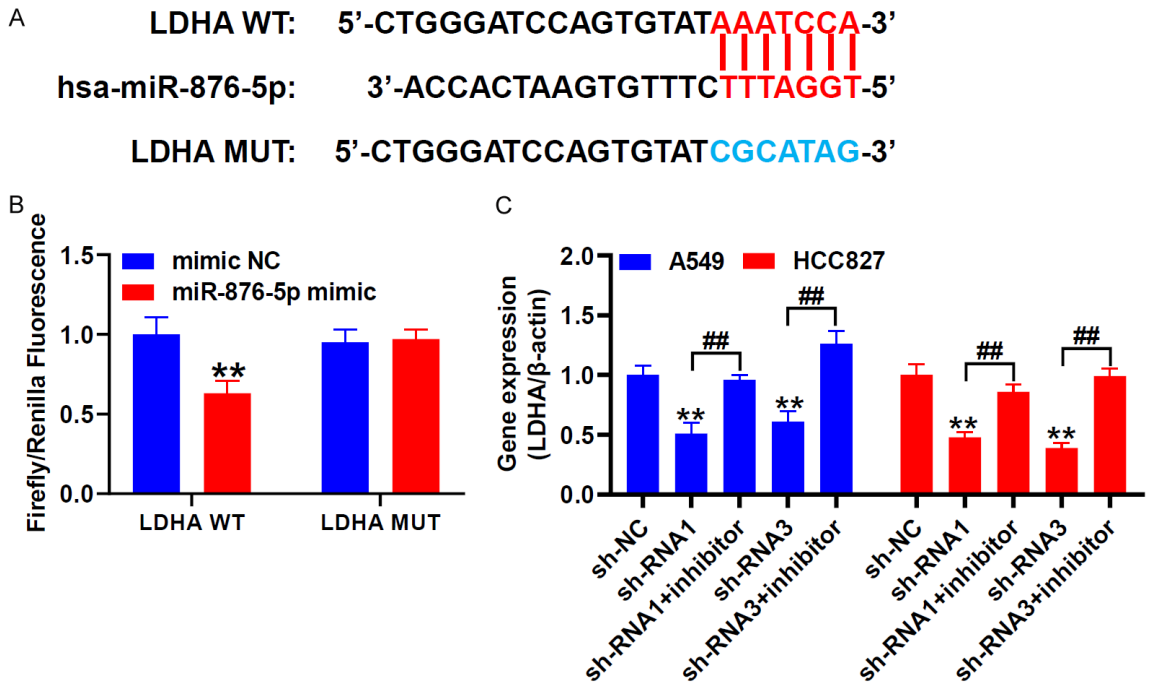

Figure S1. miR-876-5p directly targets LDHA and suppresses its expression. A. Predicted binding site between hsa-miR-876-5p and the 3'UTR of LDHA, with red text indicating the seed sequence region. The mutated sequence (LDHA MUT) disrupts miR-876-5p binding. B. Dual-luciferase reporter assay results show that miR-876-5p mimic significantly reduces luciferase activity in the LDHA-WT group but not in the LDHA-MUT group, indicating specific targeting. C. qRT-PCR analysis of LDHA mRNA expression in A549 and HCC827 cells after knockdown of hsa_circ_103089 by shRNA1 and shRNA3, with or without miR-876-5p inhibitor co-transfection. LDHA expression is suppressed by shRNA and rescued by the miR-876-5p inhibitor. Data are shown as mean ± SD from three independent experiments. **P < 0.01, compared with sh-NC group ; ##P < 0.01, compared with shRNA + inhibitor group.

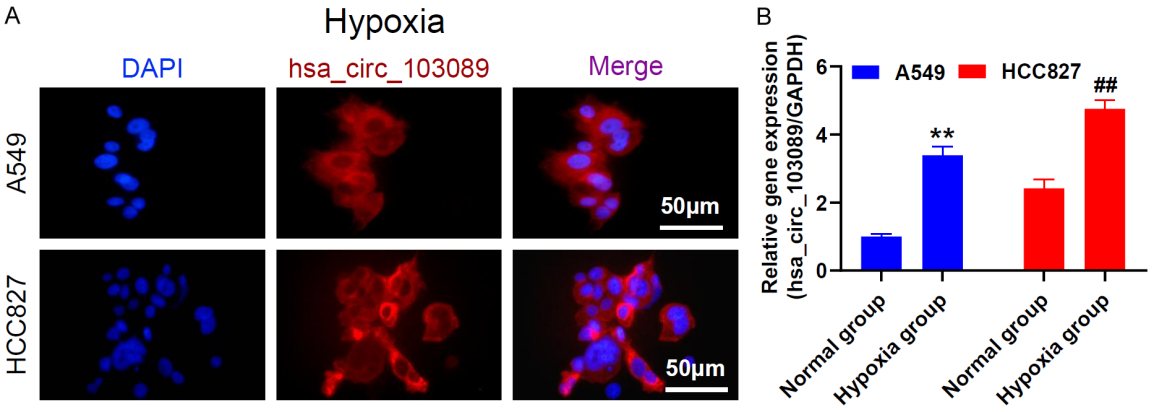

Figure S2. Hypoxia induces the upregulation of hsa_circ_103089 in NSCLC cells. A. Fluorescence in situ hybridization (FISH) was performed to detect the subcellular localization and expression level of hsa_circ_103089 under hypoxic conditions (1% O_2, 24 h) in A549 and HCC827 cells. Red fluorescence indicates hsa_circ_103089, while blue fluorescence indicates nuclear staining by DAPI. Merged images demonstrate that hsa_circ_103089 is primarily localized in the cytoplasm. Scale bars: 50 μm. B. The bar graph shows relative fluorescence intensity of hsa_circ_103089 in both cell lines under normoxia and hypoxia. Data are presented as mean ± SD (n = 3); ##P < 0.01, **P < 0.01.